2010

Influence of crosslink density on swelling and conformation of surface-constrained Poly(N-isopropylacrylamide) hydrogels

Ryan S. Cates
University of South Florida

Influence of Crosslink Density on Swelling and Conformation of Surface-Constrained Poly(N-Isopropylacrylamide) Hydrogels

by

Ryan S. Cates

A Thesis submitted in partial fulfillment
of the requirements for the degree of
Master of Science in Chemical Engineering
Department of Chemical and Biomedical Engineering
College of Engineering
University of South Florida

Major Professor: Ryan G. Toomey, Ph.D.
Nathan D. Gallant, Ph.D.
Babu Joseph, Ph.D.

Date of Approval:
March 31, 2010

Keywords: Crosslinked polymer, thermoresponsive polymers, Flory-Rehner theory, soft lithography, confocal microscopy.

TABLE OF CONTENTS

LIST OF TABLES

LIST OF FIGURES

INFLUENCE OF CROSSLINK DENSITY ON SWELLING AND CONFORMATION OF POLY(N-ISOROPYLACRYLAMIDE) HYDROGELS

Ryan Scott Cates

ABSTRACT

A stimuli-responsive microgel is a three-dimensional polymer network that is able to absorb and expel a solvent (commonly water). These materials are unique in the fact that their sponge-like behavior can be actuated by environmental cues, like temperature, ion concentration, pH, and light. Because of the dynamic properties of these materials they have found applications in drug-delivery systems, micro-assays, selective filtration, artificial muscle, and non-fouling surfaces. The most well-known stimuli-responsive polymer is Poly(N-isopropylacrylamide) or PNIPAAm and it experiences a switchable swelling or deswelling over a critical temperature ($T_c \cong 32$ °C). Below the critical temperature, the gel begins mixing with the surrounding solvent and swells; above this temperature, the opposite is true. The unconstrained hydrogel will continue to swell in all directions until equilibrium is established between its propensity for mixing with the surrounding solvent and the elastic restoring forces of the gel matrix. The strength of the elastic restoring forces is dependent on the interconnectedness of the polymer network and is therefore a function of crosslink density. An increase in crosslink density results in

a decreased swelling and vice versa. If the hydrogel is mechanically constrained to a surface, it can experience various wrinkling and buckling conformations upon swelling, as the stresses associated with its confinement are relieved. These conformation characteristics are a strong function of geometry (aspect ratio) and extent of swelling (i.e. crosslink density). In order to capitalize on the utility of this material, it is imperative that its volume transition is well characterized and understood.

Toward this end, pNIPAAm gels have been created with $1x10^{-7}$ to $2x10^{-3}$ mol/cm^3 crosslink density and characterized. This was done by first examining its bulk, unattached swelling ability and then by evaluating its microscale properties as a surface-confined monolithe. The latter was achieved through the use of confocal microscopy and copolymerization with a fluorescent monomer. This method allows for a detail analysis of the deformations experienced (bulk-structural bending and surface undulating) and will ultimately lend itself to the correlation between crosslink density and the onset of mechanical phenomena.

CHAPTER ONE: INTRODUCTION, MOTIVATION AND BACKGROUND

1.1. Introduction to Poly(N-Isopropylacrylamide)

Stimuli responsive polymers are unique materials with applications in drug-delivery agents[1], microfluidics[2-5], molecular capture and release[6], and non-fouling surfaces[7, 8]. Poly(N-isopropylacrylamide) or PNIPAAm, is the most well-known thermo-responsive hydrogel or water containing gel, which experiences a phase change, causing swelling or deswelling, over some critical temperature ($T_c \cong 32\,^{\circ}\text{C}$) [9-11]. Below the lower critical solution temperature (LCST), the gel is soluble in the surrounding solvent and the interconnected chains begin to extend and further mix with the solvent. Here the free energy of mixing (i.e. the energy that can be converted to do work) is greater than the elastic energy of the polymer chains (i.e. spring-like energy) which had previously kept the polymer matrix coiled or collapsed. Visuals of these coiled and collapsed states are provided in figure 1-1. Effectively, the driving force to mix with the solvent outweighs the forces keeping the polymer matrix collapsed. The exact reverse relationship is observed above the LCST. The swelling or deswelling of the gel matrix comes to a final equilibrium state when free energy is minimized (i.e. the two energies balance one another) [12, 13].

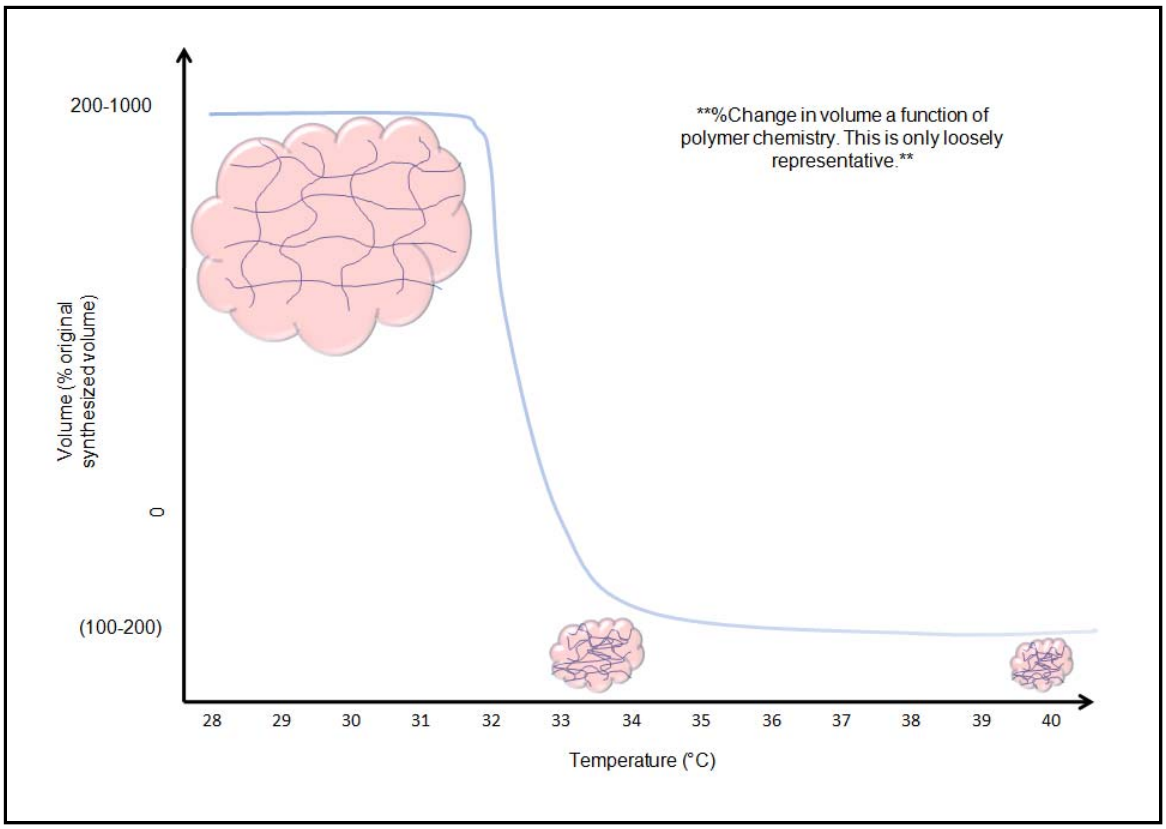

Figure 1-1: A representation of the swelling and deswelling of PNIPAAm.

PNIPAAm can take on different physical and chemical properties through copolymerization and functionalization which gives its gels application specific tunability [15]. Through copolymerization with other monomers, PNIPAAm is able to be responsive to environmental cues other than temperature. Additional, copolymerization can be used to control the threshold value of stimulus needed to induce a transition and can even alter the rate of the volume phase transition (e.g. from a highly non-linear to a linear rate).

If these PNIPAAm copolymers are to be used onboard devices and are mechanically adhered to a surface, it is found that, upon swelling, these gels assume different structural conformations as they change in size[14]. When this gel is confined to a rigid substrate and swollen, swelling primarily occurs in the direction normal to the

surface with less swelling in parallel directions[3, 15]. This is the result of limitations in solvent penetration due to surface confinement, and leads to anisotropic distribution of osmotic pressure throughout the gel and results in biaxial compressive stresses. The compressive stresses are not experienced in untethered gels and are the direct result of the immobilization of one plane of the gel[3, 15, 16]. The swelling nature of both unconfined and confined PNIPAAm gels are displayed in figures 1-2 and 1-3[17].

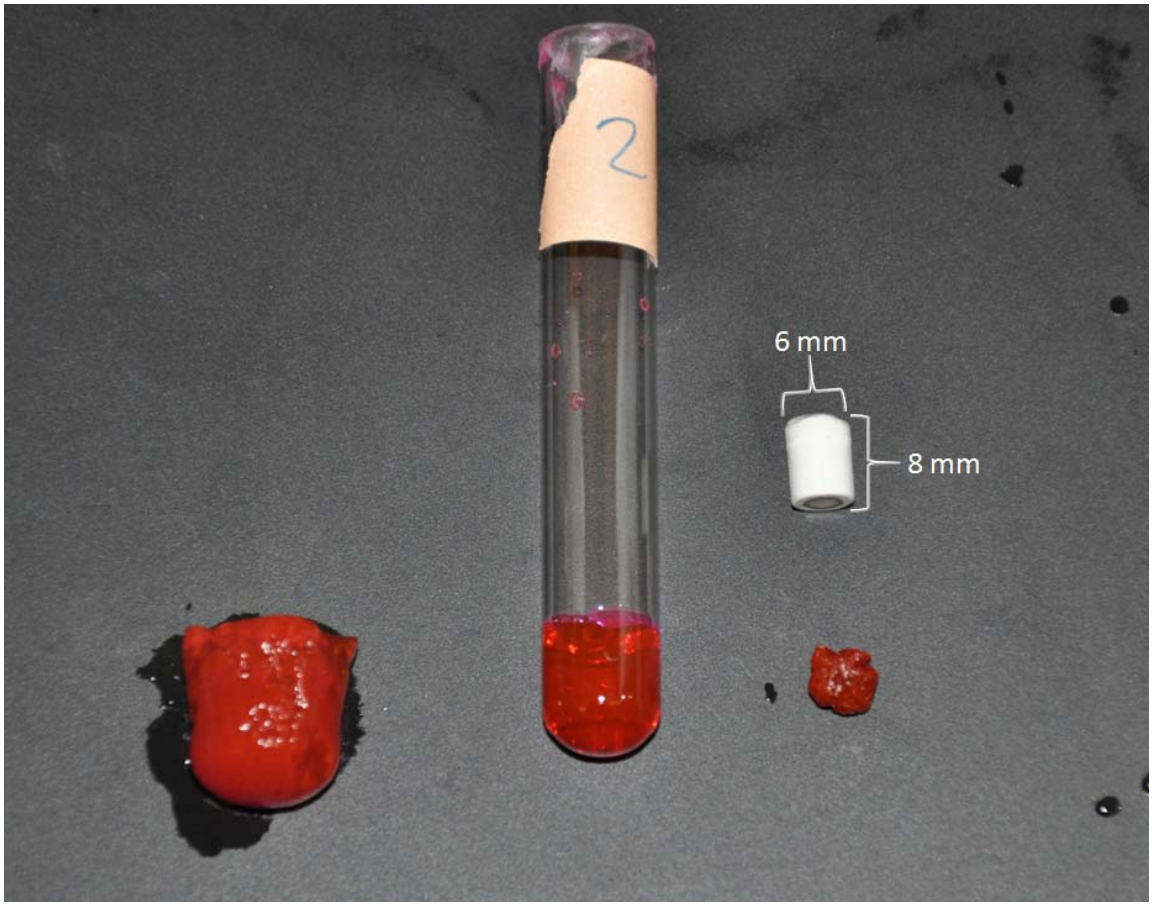

Figure 1-2: Hydrogel in three stages: fully swollen (left), after polymerization with ambient moisture content (center), fully collapsed (right). *Eraser added for size reference*

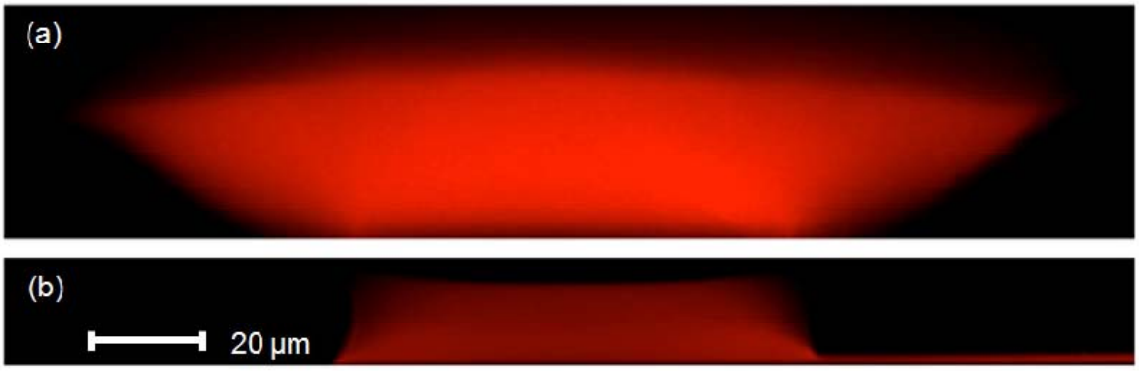

Figure 1-3: Cross-sectional profile of a surface-confined hydrogel in its swollen (a) and unswollen (b) states.

To relieve these compressive stresses, mechanical distortions in the form of surface wrinkling or edge undulating results[15, 18-20]. Additionally, it has been found that the geometry of the surface confined gel plays a significant role in determining the mechanical deformation, figure 1-4[21, 22]. In addition to geometry, the threshold and magnitude of mechanical deformations is contingent on the methods of preparation and the chemical composition of the media; including copolymers, initiators, and cross-linkers[23-25]. This dependence on crosslink density for both unconstrained and constrained PNIPAAm gels is show in figures 1-5 and 1-6.

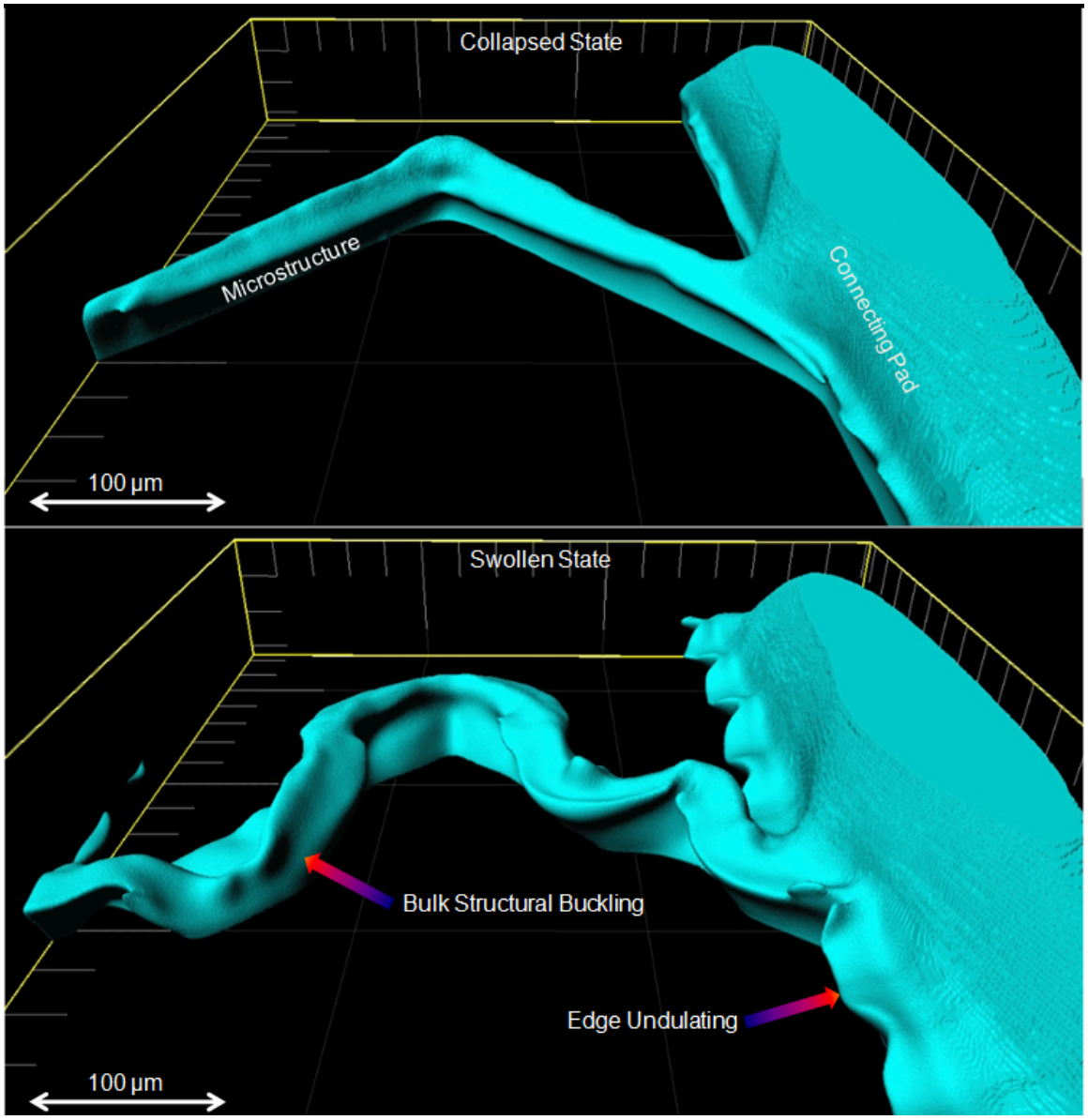

Figure 1-4: Surface confined microgel in the swollen and unswollen state. The swollen state displays mechanical deformation of the microgel.

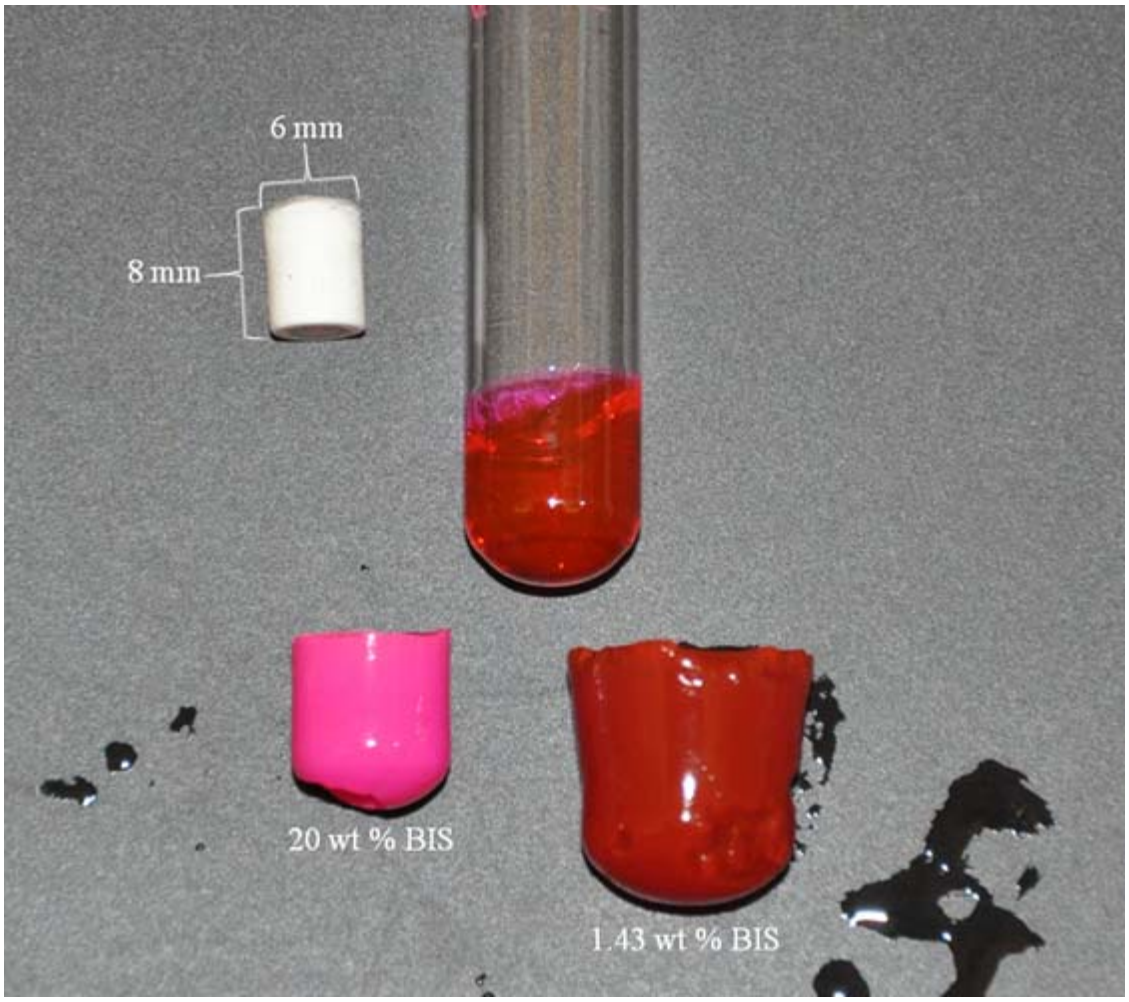

Figure 1-5: PNIPAAm samples: Fully swollen at highest crosslink density (20 wt % BIS, left), at the lowest crosslink density (1.43 wt%, right) and the initial, unswollen state (top).

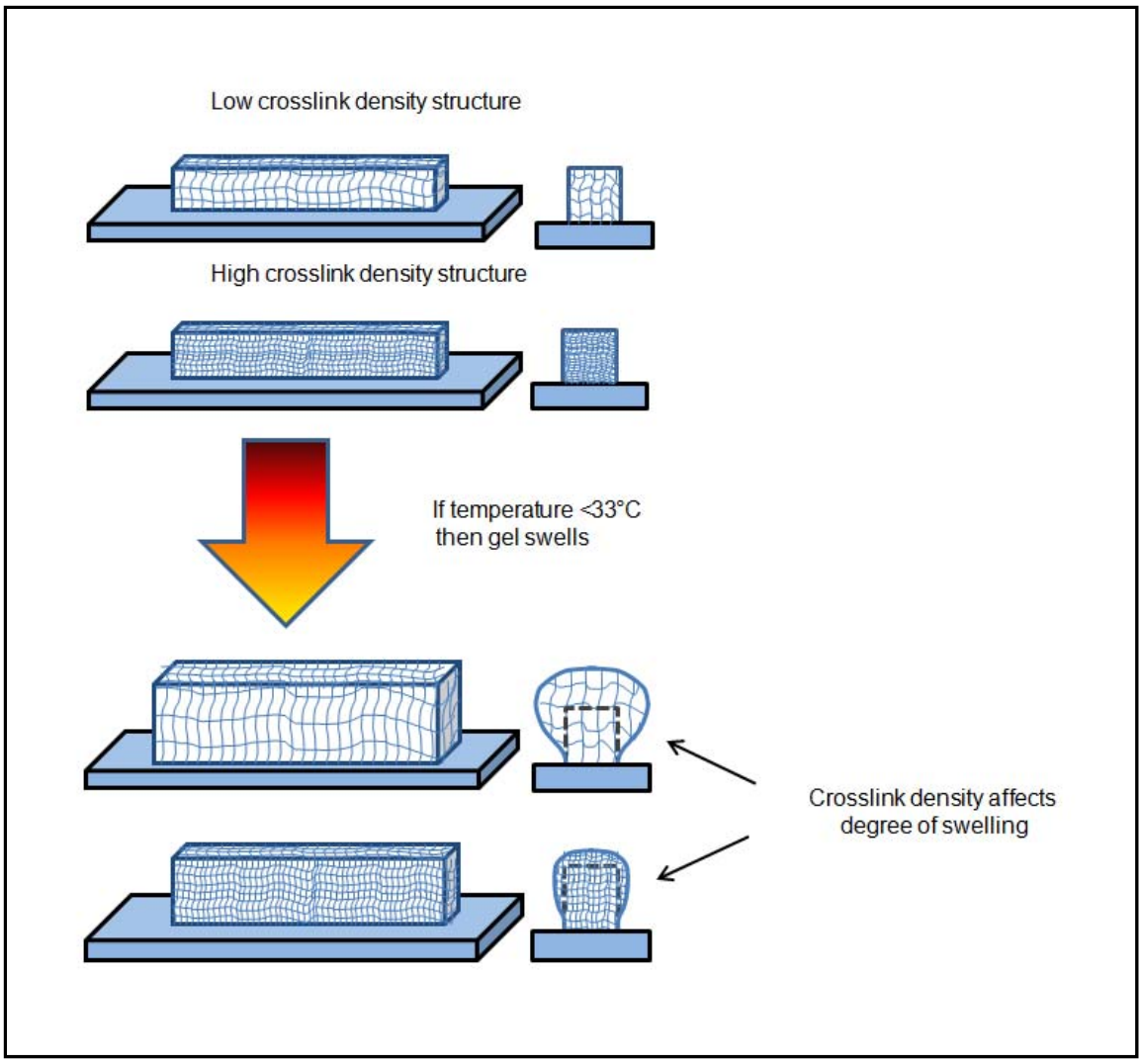

Figure 1-6: Surface-confined PNIPAAm samples swelling as a function of crosslink density.

Herein, the dependence of swelling on cross-link density is examined; first through macrogel swelling test and then in surface patterned microgels. Both gels are synthesized using a fluorescent comonomer, which will enable the characterization of the patterned microgels by confocal microscopy.

CHAPTER TWO: FABRICATION OF POLY(N-ISOPROPYLACRYLAMIDE) MICROSTRUCTURES

Traditionally high aspect ratio microstructures or those greater in height than width, have been produced by a variety of techniques including photolithography and ion etching, such as deep reactive ion etching (DRIE) or focused ion beam (FIB) techniques[26, 27]. Because the equipment to run these processes is expensive and their operation is complicated to learn (often requiring a full time technician) the widespread use of them is limited[28]. By contrast, soft lithography techniques require comparatively inexpensive equipment and are straightforward to learn and apply[28]. Additionally, soft lithography can circumvent diffraction limitations associate with projection photolithography, produce quasi three dimensional structures, create structures or patterns on non-planer surfaces, and can be used with a wide variety of surface chemistries[28]

In this study techniques from both approaches are used. Photolithography is first used to generate a silicon patterned mold that can be used to create an elastomer (soft) relief mold. SU-8 photoresist epoxy is spun onto 4” silicon wafer and patterned using a sodalime quartz / chrome photolithography mask and UV irradiation. Once these “master” molds have been fabricated the siloxane elastomer is poured over the mold to generate a relief pattern. The photolithographic process is outline in the flow diagram in figure 2-1. This relief pattern is then used in a micro injection molding in capillary (MIMIC) technique to fabricate patterned, PNIPAAm microstructures. Additional surface treatments are also used to chemically adhere the structures to the substrate surface.

Using both techniques, allows for easy, repeatable fabrication of “soft” molds and a patterning process that may be carried out in an ordinary laboratory.

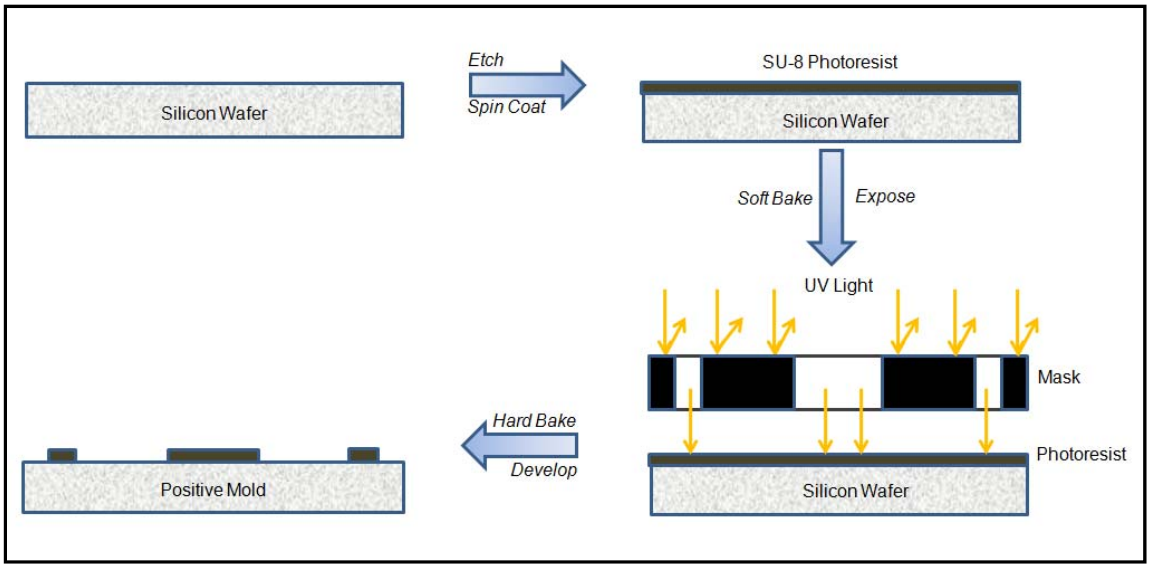

Figure 2-1: Photolithography process.

2.1 Creation of Photolithographic Mask Using AutoCAD

Over the course of this investigation two masks were designed (Monolithe I and II) in AutoCAD and manufactured by Advanced Reproductions, Inc. These mask were created with the known physical properties and limitation of SU-8 photoresist, PDMS and PNIPAAm in mind and were tailored to investigate unknown or poorly understood phenomena of PNIPAAm microstructures.

2.1.1. Monolithe I

Monolthe I was designed based on the results from the previously used photolithography mask, which yielded microgel monolith structures that displayed buck out-of-plane bending and edge undulations and cylindrical microgels that showed in-plane twisting upon swelling. More information was desired from these two shapes

regarding all of these phenomena and they were included in greater geometric variety in Monolithe I. Additionally these structures were spaced more liberally from one another to avoid problems with underdevelopment and PDMS fouling in the trenches between adjacent microstructures, shown in figure 2-2.

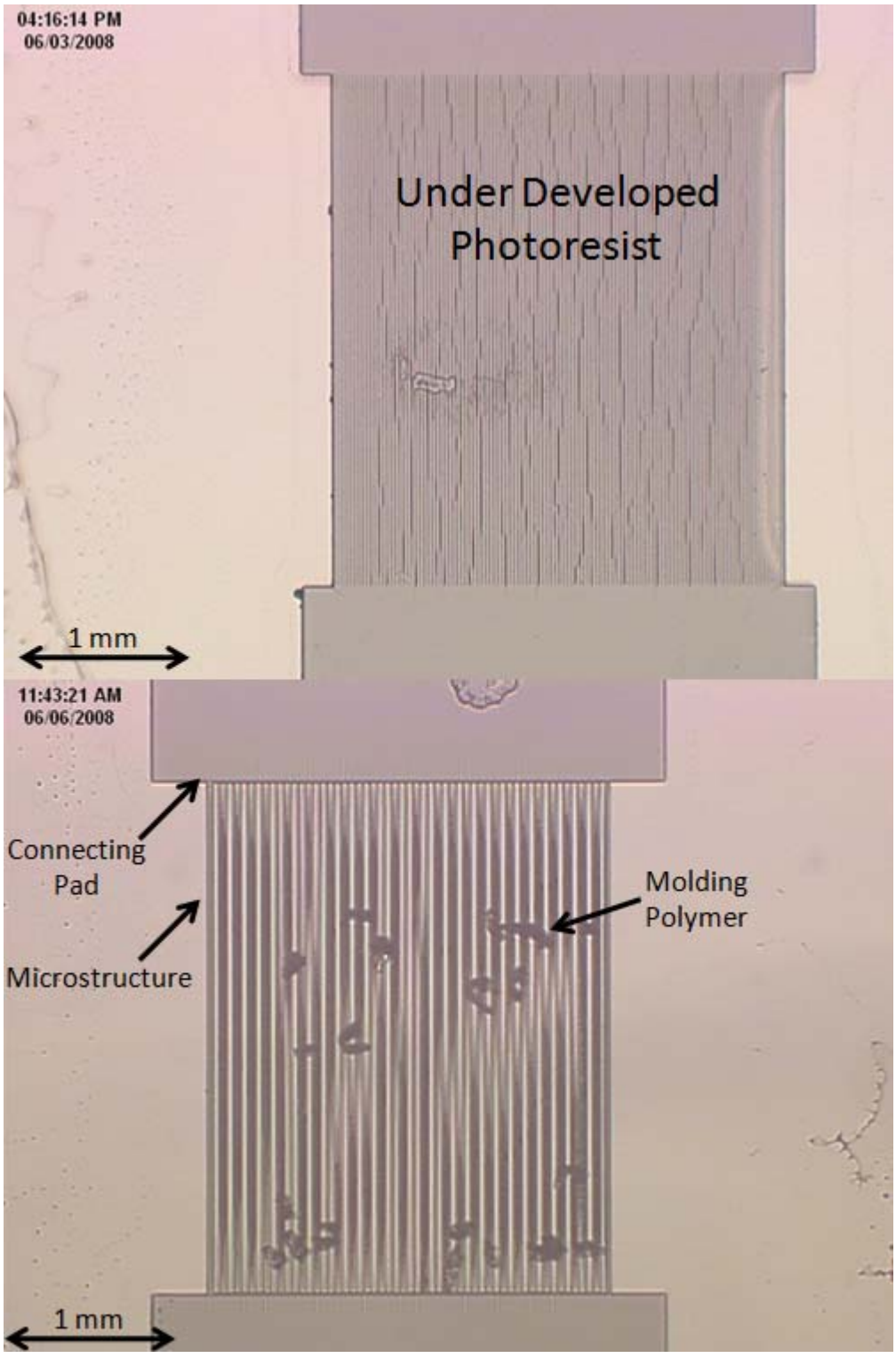

Figure 2-2: Underdeveloped photoresist pattern and the trapping of the molding polymer.

This mask was designed to investigate the affect that width, length and curvature had on the surface-confined swelling of monolithe structures and how diameter and arc length altered the swelling of surface confined cylindrical structures. To this end, the following structures were designed: single beams varying in length (100 μm to 5 mm) and width (5 μm – 100 μm), single waves varying lengths (1 mm & 3 mm), arc angles (10° - 90°) and periodicities (1 – 3), single saw waves varying in length (200 & 400 μm), width (5 μm – 100 μm) and periodicity (1 – 4), and circles varying in diameter (0.5 mm & 1.5 mm), arc angle (5° - 180°), and periodicity (1-4). A full schematic of this design is displayed in figure 2-3 and its key in table 2-1.

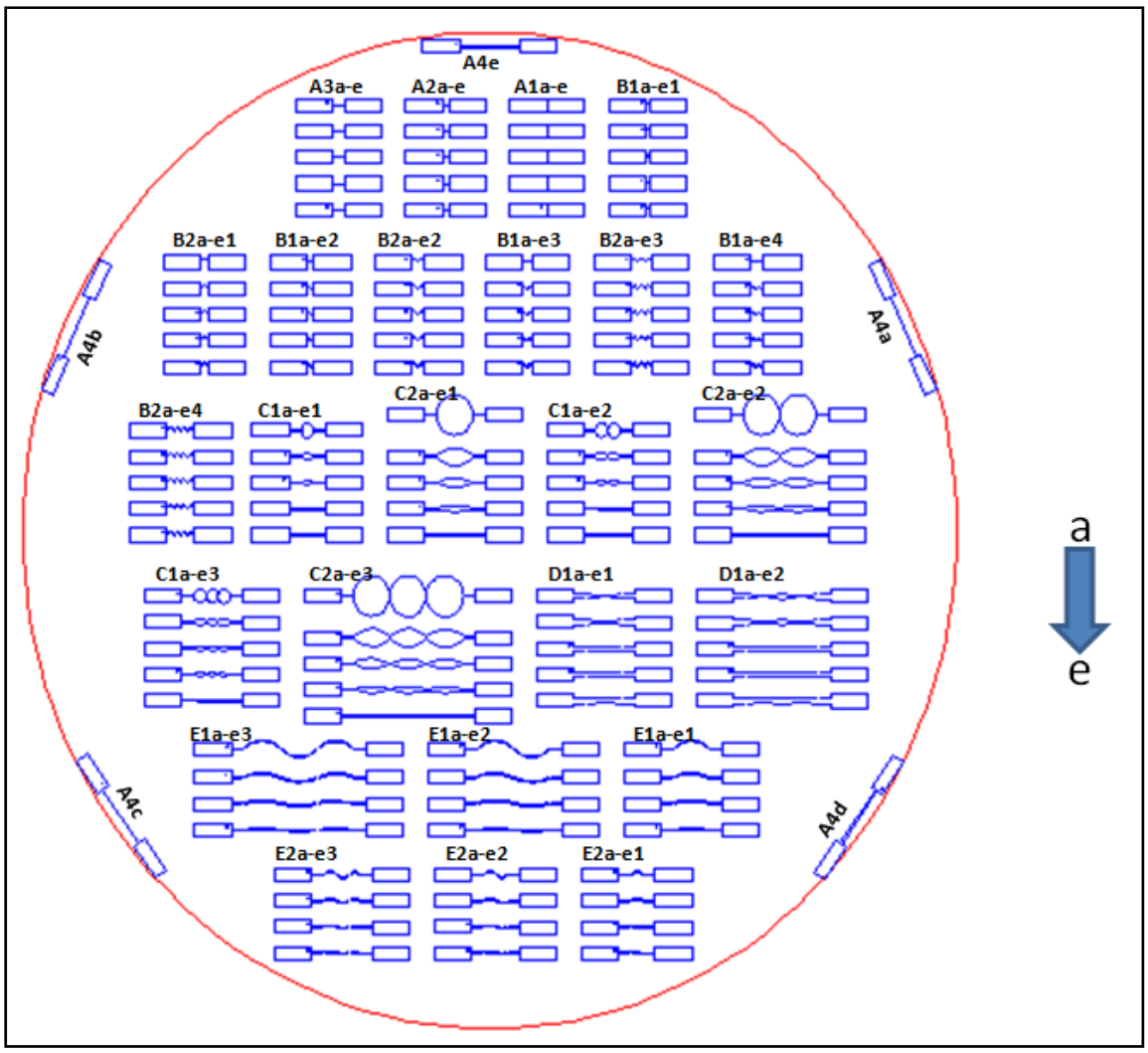

Figure 2-3: AutoCAD schematic of the “Monolithe I” photolithographic mask.

Table 2-1: Dimensions key for Monolithe I schematic.

Structure	Dimensions (μm)	Structure	Dimensions (μm)
Axy		*Dxyz*	
x=1-4 (length)	100.500.1000.5000	x=1 (length)	3000
y=a-e (width)	5.10.20.50.100	y=a-e (Arc Angle)	25.20.15.10.5
Bxyz		z=1-2 (Periodicity)	1.2
x=1-2 (length)	200.400.	*Exyz*	
y=a-e (width)	5.10.20.50.100	x=1-2 (length)	1000.3000.
z=1-4 (Periodicity)	1.2.3.4	y=a-d (Arc Angle)	90.50.25.10
Cxyz		z=1-3 (Periodicity)	1.2.3
x=1-2 (Diameter)	500.1500.		
y=a-e (Arc Angle)	180.90.50.25.5		
z=1-3 (Periodicity)	1.2.3		

2.1.2. Monolithe II

Monolithe II was design to further investigate the unique properties of single, linear, surface-confined structures and to speed up the production of these samples, through the creation of battery groups. These groups included single, constant width monolithes ranging from 5-100 μm, monolithes descending in width from 100-5, 100-10, 60-4, 40-20 and monolithes that descend and then ascend to their original width. With the remaining mask space, patterns for creating low aspect ratio bar structures with different geometric pits, and free standing doughnut structures were designed to look at potential encapsulation applications. Lastly, single lines of text were also worked into the design. An AutoCAD drawn schematic of Monolithe II is shown in figure 2-4 and a close-up of a select structure in displayed figure 2-5.

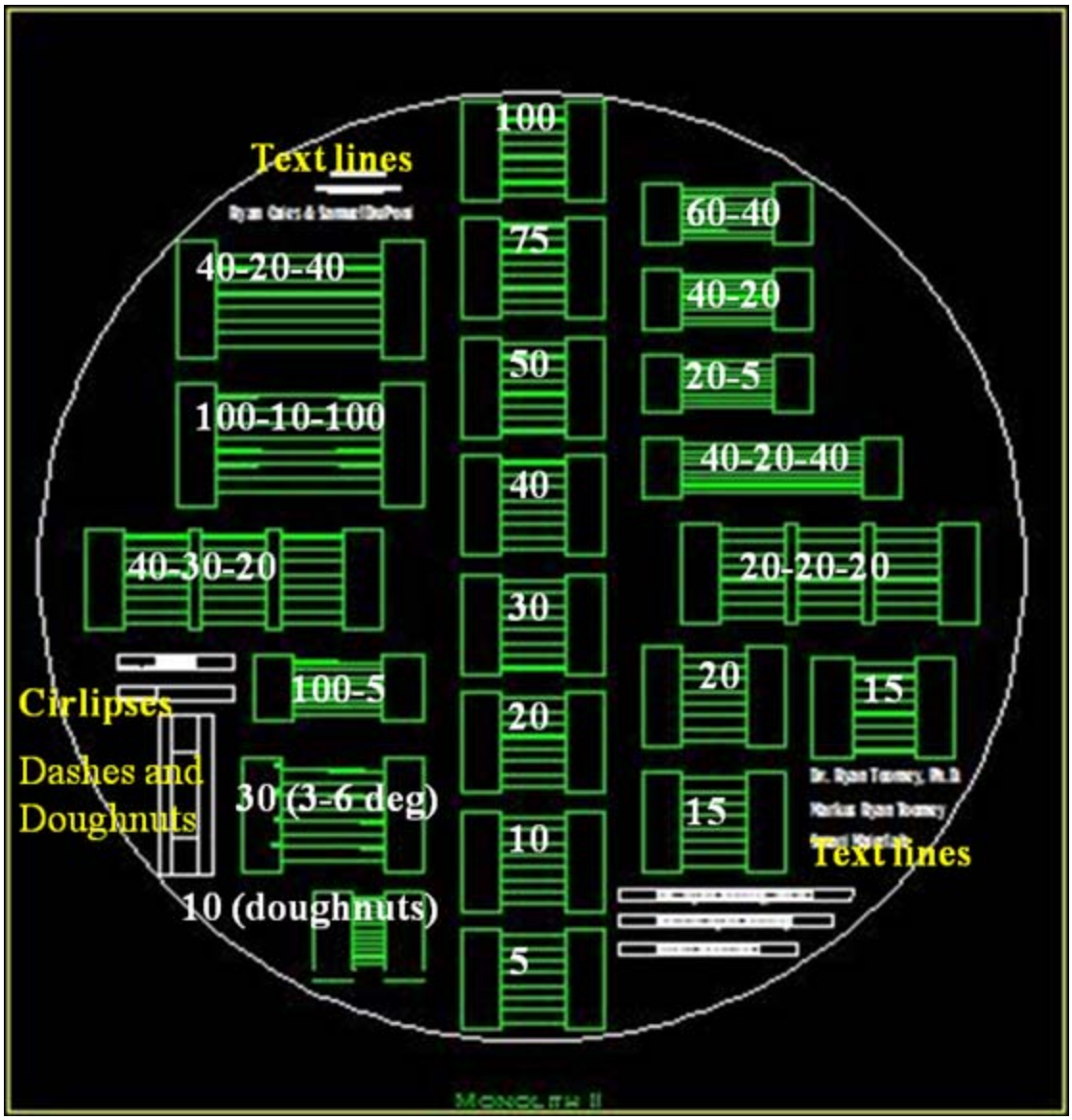

Figure 2-4: AutoCAD schematic of “Monolithe II” photolithographic mask.

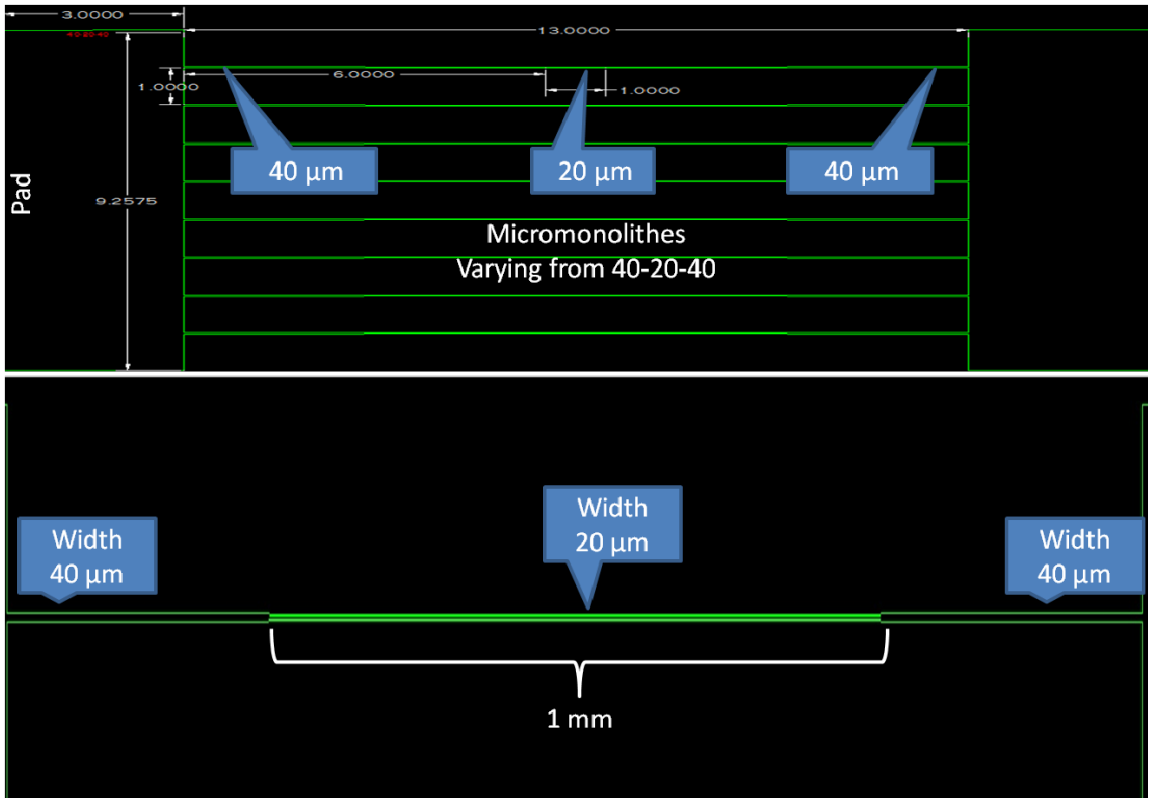

Figure 2-5: Close-up of the 40x20x40 µm structure on the AutoCAD schematic of the "Monolithe II" photolithographic mask.

2.2. Photolithography Process

To achieve different aspect ratios, the thickness of the SU-8 micromolds (height of the photoresist) was varied by different SPIN speeds and photoresist viscosity. Photoresists SU-8 3025, SU-8 2035 or SU-8 100 were used to achieve photoresist thicknesses of 25-50 µm, 40-70 µm and 80-100 µm samples respectively.

2.2.1. Piranha Clean

Before beginning the photolithography process, it is important that the silicon substrate is cleared of all impurities to insure proper adhesion of the photoresist.

One way by which this is accomplished is through wet etching, in this case a Piranha etch. This was accomplished by using a solution of H_2SO_4 and H_2O_2 (3:1 volume ratio) which produces a very exothermic oxidation reaction[29-31]. This solution is capable of removing organic residues and hydroxylating the substrate's surface, all without altering surface topography[29-31]. Because of the differences in density and the tendency of acid to flash boil when mixed incorrectly, it is advised that the sulfuric acid is added to the hydrogen peroxide and that all of this is performed with extensive PPE (e.g. a face mask, chemical resistant gloves and apron) [29]. In most microprocessing clean rooms, this process is performed on a well ventilated hood because of the possibility of noxious products and because of the exothermic nature of this reaction.

Once the Piranha solution is mixed, the n-type, single-side polished 4" silicon wafers were added and allowed to etch for 15 minutes. At the end of 15 minutes, the reaction was slowed to a stop by dilution with a constant stream of de-ionized water (DI water) for approximately 5 minutes. From here the wafers were removed, further rinsed with DI and dried by a continuous flow of nitrogen. To insure all residual water was removed and would not interfere with the future photoresist film, the wafers were further dried by a dehydration bake for 30 minutes at 250°C.

2.2.3. Photoresist Application

In order to achieve a uniform coating of photoresist across the surface of the wafer, a spin coating technique was used. Different film thicknesses were achieved by varying the viscosity of the photoresist, SU-8, and by using different spin recipes recommended by the manufacturer, MicroChem. SU-8 was chosen because of its high optical transmission, its ability to reliably reproduce high aspect ratio, high resolution structure (+/- 5 μm) and for its ease of coating. For smaller features (those <5 μm), other

techniques such as, Deep Reactive Ion Etching or Focus Ion Beam, could be used. A Model P6700 spin coater was used for photoresist application.

Spin coating regime suggested by MicroChem[32]:

- Dispense: 1 ml of photoresist per inch of wafer diameter on top of wafer-spin coater setup.
- Start-up: Start spin process at 500 RPM for 5-10 seconds (5 seconds used) with an acceleration of 100 rpm/second. This cycle is responsible for the initial spreading of the photoresist.
- Spread cycle: Begin the spread cycle at the recommended speed and duration at 300 rpm/second. Speeds and durations are provided by MicroChem.

Table 2-2 list some of the recipes used for SU-8 application and the resulting structure heights.

Table 2-2: SU-8 Spin recipes used and the results achieved

SU-8	Thickness Goal (μm)	Spread Speed (RPM)	Spin Speed (sec @ RPM)	Achieved Height (μm)
2035	35	10 @ 500	35 @ 4000	32
2035	45	10 @ 500	35 @ 3200	45
100	100	10 @ 500	35 @ 3000	80

It was found that dispensing the photoresist from the vendor's (MicroChem) container (i.e. as opposed to the use of eyedroppers pipettes or other containers) kept at room temperature and un-stirred prevented most common application defect. These defects included bubbles, spider webs (uneven, often stringing spreading) and severe edge beads. The age of the SU-8 was also a major factor in the consistency of large

batches of wafers. All this was accounted for in the end with profile characterization. In order to correct for edge beading, a cotton swab coated with photoresist developer was used to remove any excess photoresist. The soft bake directly followed to facilitate solvent evaporation and reflowing of the SU-8.

2.2.4. Soft Bake

After the photoresist application, the sample was heated on a hot plate in accordance with the vendor's specification in Table 2-3.

Table 2-3: Recommended soft bake times for different SU-8 thicknesses.

SU-8 Product	Thickness (μm)	Recommended Prebake Time @65°C (Min)	Recommended Soft Bake Time @65°C (Min)
2025	35	3	6
2035	45	3	6
100	100	20	50

Heating the sample before exposing it allows for the photoresist to reflow and compensate for any non-uniformities in the applied film. it is imperative that the hot plate is level and is placed on a level surface to prevent variation in structure height[32]. The vendor also advises against using a convection oven as this could lead to the formation of a skin on the photoresist, which could further blemish results[32].

2.2.5. Exposure

The photomasks discussed above were used to selectively block UV light from reaching the sample's surface, thereby preferentially crosslinking portions of the

photoresist film. To achieve this, a Carl Suss Mask Aligner was used and the samples were illuminated for periods of time that varied as a function of light intensity and were dictated by photoresist type and thickness. The samples were actually dosed with 125% of the prescribed values of the vendor to insure complete developing, as problems with underdevelopment were experienced following their prescription verbatim. In Table 2- 4 a list of exposure amounts can be found for all pertinent samples.

Table 2-4: 125% of the recommended UV dosages for different SU-8s and desired thicknesses.

SU-8 Product	Thickness (μm)	Recommended UV Dosage (mJ/cm^2)	Exposure Time (Sec.) Lamp Output [39 mW/cm^2]
2025	30	155	10
2035	45	160	10
100	100	240	15

To screen out UV radiation below 350 nm of wavelength, a Hoya UV-34 filter was used. It is important to limit the amount of high intensity UV radiation because it has the propensity to cause overdevelopment of the superficial layers of the photoresist, resulting in uneven sidewalls or “T-topping” upon developing[5]. To further increase pattern resolution, the photoresist/photomask separation distance was minimized to reduce errors resulting from diffraction[33]. This technique was also cited by Revzin (2001) who found that the minimum resolution is directly proportional to the square root of the photoresist/photomask separation distance[34].

Due to separation distance imposed by an unlevel photoresist film, variation in height and structure resolution were seen in all samples, In the future this could be

further avoided by using a technique developed by Chuang (2002), whereby glycerol is placed in the photoresist/photomask gaps to reduce Fresnel diffraction[33].

2.2.6. Hard Bake

After exposing the sample, a post exposure hard bake was performed in accordance with the vendor's recommendation. During this time, the appearance of the photomask image was used as confirmation that the sample was given an ample UV dosage to develop the photoresist. In Table 2-5, a list bake times and temperatures can be found for all pertinent samples.

Table 2-5: Post exposure bake times recommended by Microchem Corp. for different SU-8 samples and thicknesses.

SU-8 Product	Thickness (μm)	Bake Time (Min) @ (65°C)	Bake Time (Min) @ (65°C)
2025	30	1	6
2035	45	1	6
100	100	1	12

These samples were allowed to return to room temperature before being developed

2.2.7. Development

All samples were developed in a shallow Pyrex dish under gentle agitation for the amount of time recommended by the vendor[32]. The developer used was a proprietary SU-8 photoresist developer provided by MicroChem. After the prescribed time, the sample was removed from the developer and rinsed with lab grade isopropyl alcohol, IPA, to quench the developing reaction and to test for completion. If a white film resulted, this indicated incomplete developing and additional time was given. Once the sample

finished developing, it was removed and rinsed with IPA and DI water and then dried with a stream of nitrogen. In table 2-6 a list developing times can be found for all pertinent samples.

Table 2-6: Developing times for different SU-8 samples and thicknesses.

SU-8 Product	Thickness (μm)	Developing time (min.)
2025	30	6.5
2035	45	7
100	100	15

When working with large structures or those with high aspect ratios, it is important to use caution when using nitrogen streams to dry the sample, as the high pressure could delaminate the SU-8 structures.

2.2.8. Characterization

After developing the microstructures, all samples were examined under a light microscope to check for broken patterns or other irregularities. If a sample was too badly marred or was not to specification, the SU-8 was removed by Reactive ion etching at 100 mTorr and 10°C with 200 W with 80 sccm O_2 and 8 sccm CF_4. To verify the microstructure heights, a Tencor Alphastep 200 Profilometer was used.

2.2.9. Extended Hard Bake

Per recommendation of the vendor, the final samples were heated on a hot plate to 200 °C for a period of approximately thirty minutes. In past attempts to use SU-8 microstructures as master molds for soft lithography, delamination of the SU-8 has been an issue. This final annealing step increases the strength of the mold thereby decreasing

the likelihood of delamination. After heating, the samples were allowed to return to room temperature on the hotplate to avoid thermal shocking.

2.3. Soft Lithography

Soft lithography is a non-photolithographic field that is founded on self-assembly and mold casting over patterned relief structures for the fabrication of structures ranging from 30 nm to 100 μm[28, 35]. Microcontact printing (μCP), replica molding (REM), solvent-assisted micromolding (SAMIM), microtransfer molding (μTM) and micromolding in capillaries (MIMIC) are the most prevalent staple techniques of soft lithography[28, 35]. With one or multiple of these techniques three-dimensional microstructures can be built, often even stacked layer-by-layer, to give rise to such micro devices as: mixers[36], fluidic channels[37], valves[38], pumps[39], and tweezers[40].

At the center of all of these methods, the patterned elastomeric block material must be selected according to the materials that are to be patterned. These materials include: unsensitized polymers (e.g. polyurethane, polyethylene, epoxy, etc.), colloidal materials and biological macromolecules[28]. Poly(dimethylsiloxane), PDMS, is a prevalent patterned block material because of its ease of processing, relative inexpensive and favorable chemical characteristics[28]. In addition to being biocompatible, which makes PDMS ideal for patterning proteins and cells, it is permeable to gases, optically transparent to about 300 nm, and can coat small surface features with relatively high fidelity (~+/- 5 μM) [40, 41]. The elasticity of cured PDMS, in conjunction with its low interfacial surface energy (21.6×10^{-3} Jm^{-2}) and chemically inert nature, allow for an easy removal of the patterned block from complicated and fragile positive reliefs. Lastly, PDMS is not hydroscopic and will not swell in ambient humidity

and is very durable, which allows for repeated use (50+ stampings) over a several month span without significant loss in structural fidelity[28].

While PDMS has many favorable characteristics for its application as a patterned relief mold, it is not without its drawbacks and limitations. While the elasticity and interfacial surface energy are favorable, PDMS still imposes mechanical stress on photoresist microstructures, especially those of a high aspect ratio, and can delaminate or otherwise destroy these microstructures. We have observed that in small features of the photoresist microstructures (<~10μm), the PDMS will flow and polymerize but may sometimes tear away from the bulk relief mold upon liftoff. This lowers the fidelity of the relief mold and potentially fills in small features on the photoresist pattern. Also, upon curing there is a loss in volume of the PDMS, as it will shrink about 1%[28]. This affect is noteworthy but not significant to the microstructure fidelity. Furthermore, adhesive, capillary and gravitational forces impose stresses on the PDMS stamp, causing the patterns to collapse or bow and thus produce defective prints[39]. Such defects are a strong function of geometry. Delamarche (1997) notes that the aspect ratio in these PDMS relief stamps must be within 0.2 and 2 in order to achieve defect free stamps[39].

The photolithography process discussed above, was used to generate SU-8 patterned structures that serve as the positive mold for the PDMS stamp. PDMS prepolymer solutions were mixed from two parts, an elastomeric base and curing agent, in a 10:1 ratio, respectively. This prepolymer solution was then placed under vacuum (101.6 mm Hg) until all air bubbles were removed. This ensures complete mixing of the two prepolymer constituents and prevents air bubbles from coming in contact with the positive relief surface, thus causing pockets and other imperfections in the PDMS mold, as show in figure 2-6[28]. This prepolymer mixture was then poured over the SU-8 patterned wafer and heated at 75°C for 60 minutes to cure the PDMS. Directly afterwards, the PDMS/wafer sample was removed, briefly allowed to return to room

temperature and then the PDMS was removed from the wafer. It is important that these PDMS molds are removed from the wafer in the direction of the length of the SU-8 structures to prevent delamination of these structures. Leaving the PDMS on the wafer for extended periods of time allows for the PDMS to further cure and lose more of its elasticity. We have found that this increases the likelihood of damaging SU-8 patters, especially those of high aspect ratio, and therefore such practice is avoided. At this point, the PDMS molds are placed face down on a clean, dust-free, cutting surface and cut with an Exacto knife. A Petri dish was used as both a stencil for cutting and a container for storing. This is done so that the samples may be labeled and stored in a place where they are least likely to pick up dust or other particulate matter that may compromise the molds integrity. Later these samples will be revisited and structures of interest can be cut directly out of the PDMS without removing it from the Petri dish, as shown in figure 2-7.

Figure 2-6: Air bubbles in a PDMS stamp still on an SU-8 master mold.

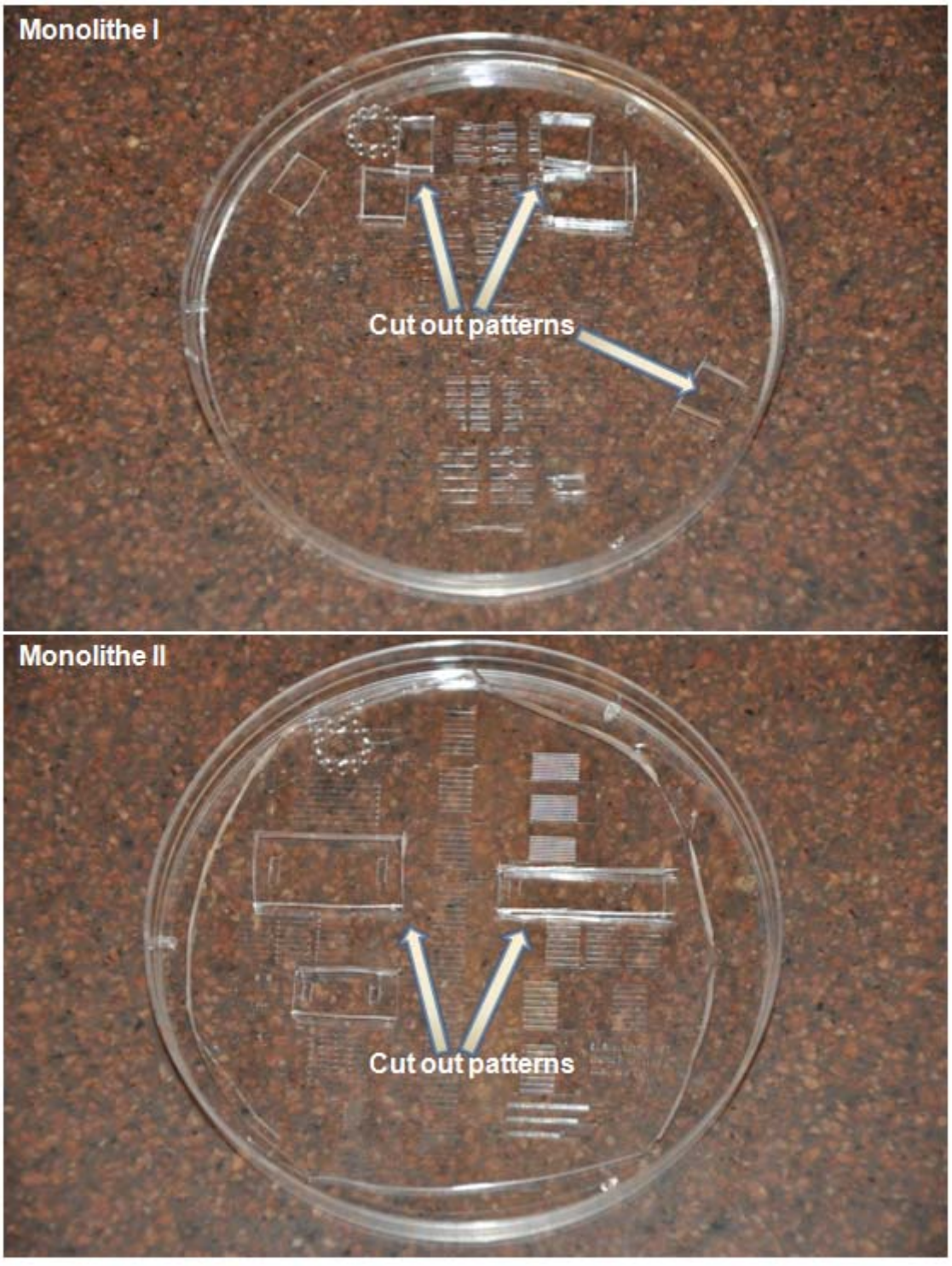

Figure 2-7: PDMS relief in petri dish.

2.3.1. Micro Molding in Capillary (MIMIC)

In MIMIC, the PDMS relief molds are placed, patterned side down, onto a substrate which forms a series of empty corridors[42]. At the open end of these corridors, a prepolymer solution is pooled and capillary forces pull the fluid through the corridors. Here the polymer is cured and the PDMS relief is removed, leaving behind the patterned polymer microstructures. It is important to note that the PDMS should be removed in the direction that runs with the length of the microstructures to prevent damaging the tops of thin structures. The entire MIMIC process is shown in figure 2-8.

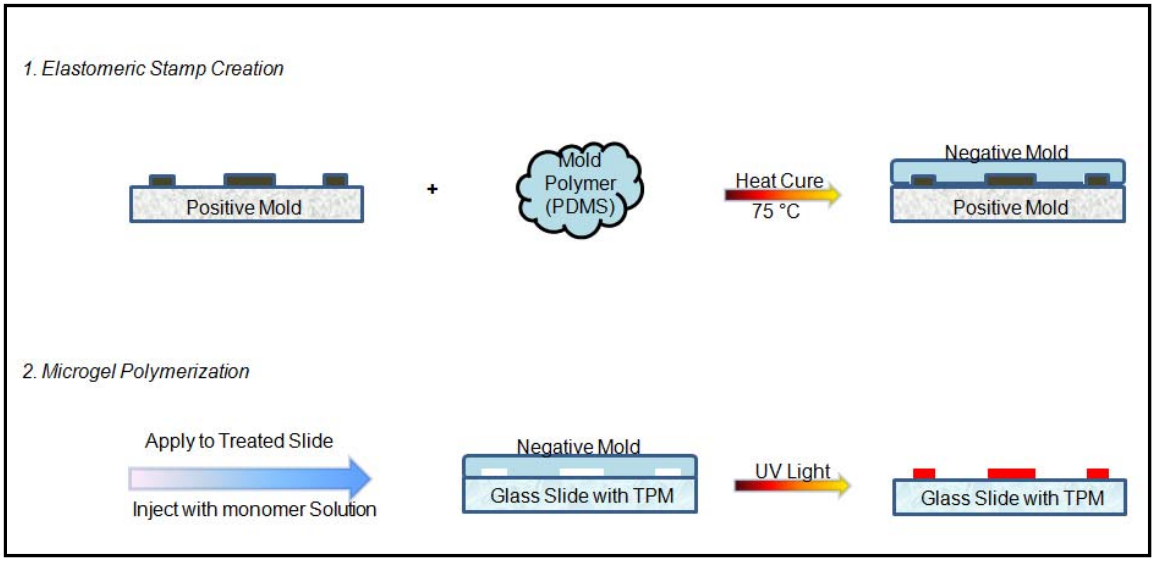

Figure 2-8: Micro injection molding in capillaries (MIMIC) process.

2.4. Application of Silane Binder to Substrate

In early attempts to deposit PNIPAAm structures onto glass surfaces, only rudimentary cleaning methods were used (acetone/methanol/isopropanol) but no fixatives were applied to the surfaces. The patterns could be cured on these surfaces and the small forces present were sufficient to adhere them to the surface, however,

when these structures swelled those weak forces were easily overcome and delamination often occurred. In response to this, all future surfaces were chemical enhanced with 3-(trichlorosilyl)propyl methacrylate (TPM, Aldrich). This self-assembled monolayer covalently bound the pNIPAAm microstructures to the glass slide during photopolymerization.

In the field of self-assembled monolayers (SAMs), chlorosilanes or alkoxysilanes are employed on silica or glass substrates to achieve dense, thick (~22 Å) monolayers with less surface roughness[43, 44]. Using a similar approach, glass cover slips (~0.170μm thick) were treated with a monolayer of TPM to give it adhesive properties[45]. In summary, the cover slides were first cleaned using a standard solvent rinse of methanol/acetone/isopropanol/DI water and then dried with high purity dry nitrogen. Subsequently, the slides were further cleaned with O_2 plasma in a Harrick Plasma Cleaner/Sterilizer PDC-32G for 15 minutes at approximately 500 mTorr of pressure and at 6.8 Watts of RF power. Plasma cleaning removes any residual organic deposits by chemical reaction with highly reactive oxygen radicals and removal by oxygen ions and promotes hydroxylation (formation of OH groups) of the surface which will help with monolayer application. From here the glass slides were treated in 3 chemical baths in glove bag, which provided an oxygen free environment. These slides were first treated for 5 minutes in a 1 mM solution of TPM in a 4:1 ratio of heptane to carbon tetrachloride at room temperature and atmospheric pressure. This was followed by subsequent soaking in hexane and then in DI water; each for 5 minutes. The mechanism for silanization is shown in figure 2-9.

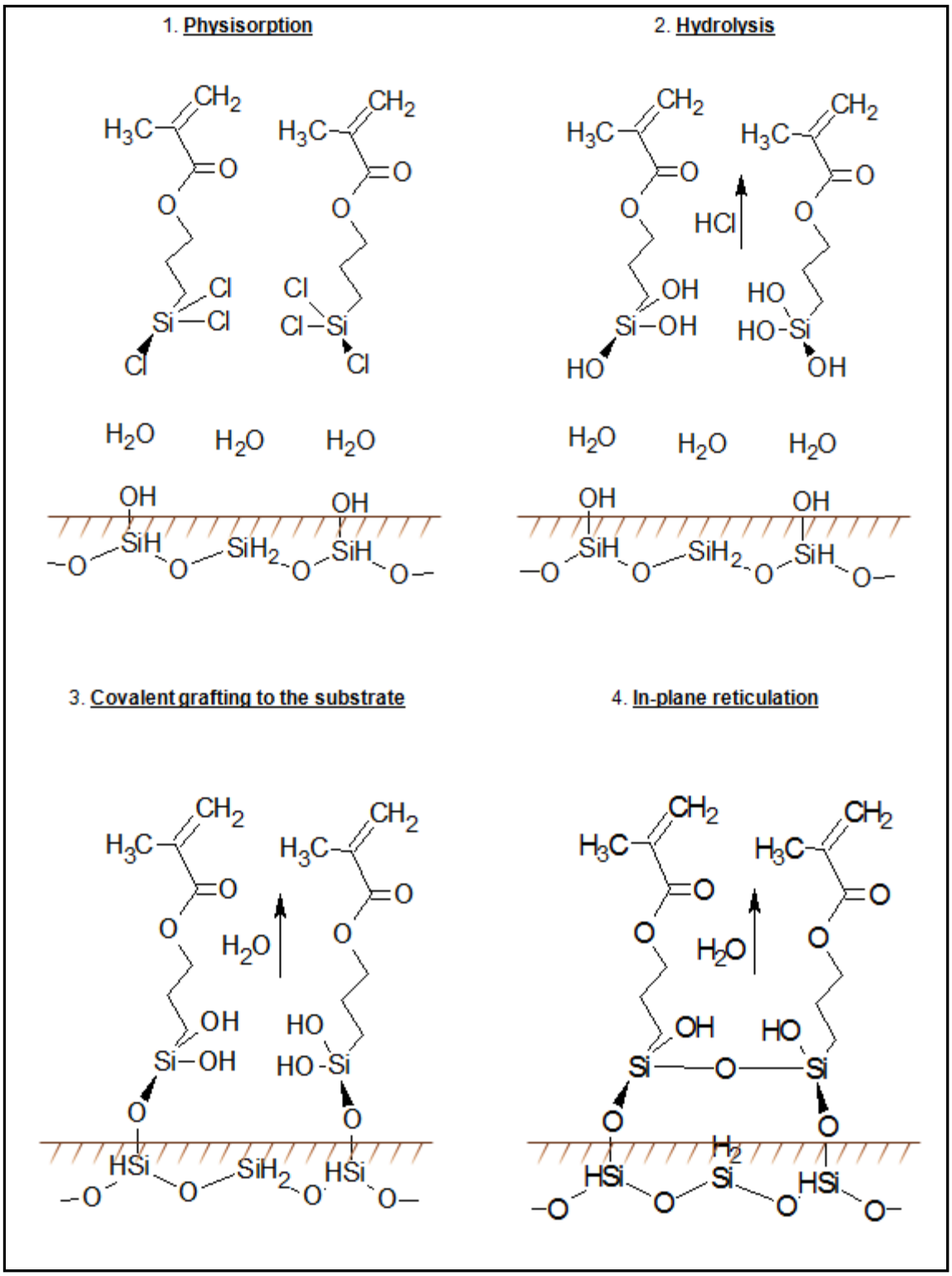

Figure 2-9: Silanization mechanism.

It was found that if too much time passed between plasma cleaning and TPM application or if precautions were not taken to ensure that samples were kept in closed, clean containers and free of particulates, that a snowing effect could be expected when the TPM was applied. This effect, shown in figure, is speculated to be indicative of thicker deposition of TPM, as shown in figure 2-10. Use of these slides with MIMIC, yields poor adhesion between the patterned PDMS mold and the substrate, which leads to the creation of scum layers (polymer that seeps under the mold and polymerizes). This is shown in figures 2-11 and 2-12. Also, if silanized slides were not used immediately (usually within a few day) the likelihood of structure delamination seemed to increase.

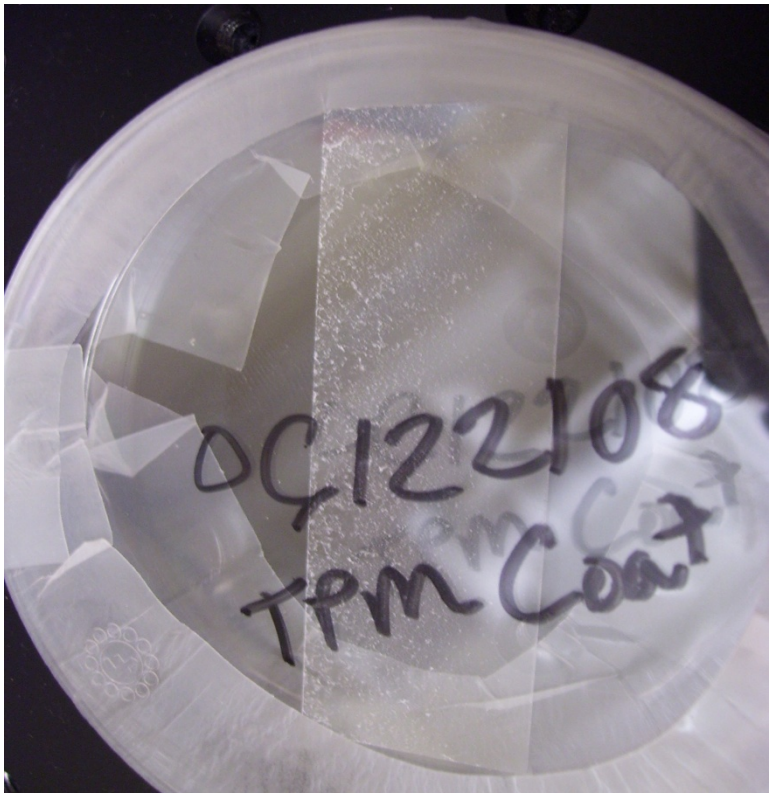

Figure 2-10: Dirty slide leading to heavy silane deposition.

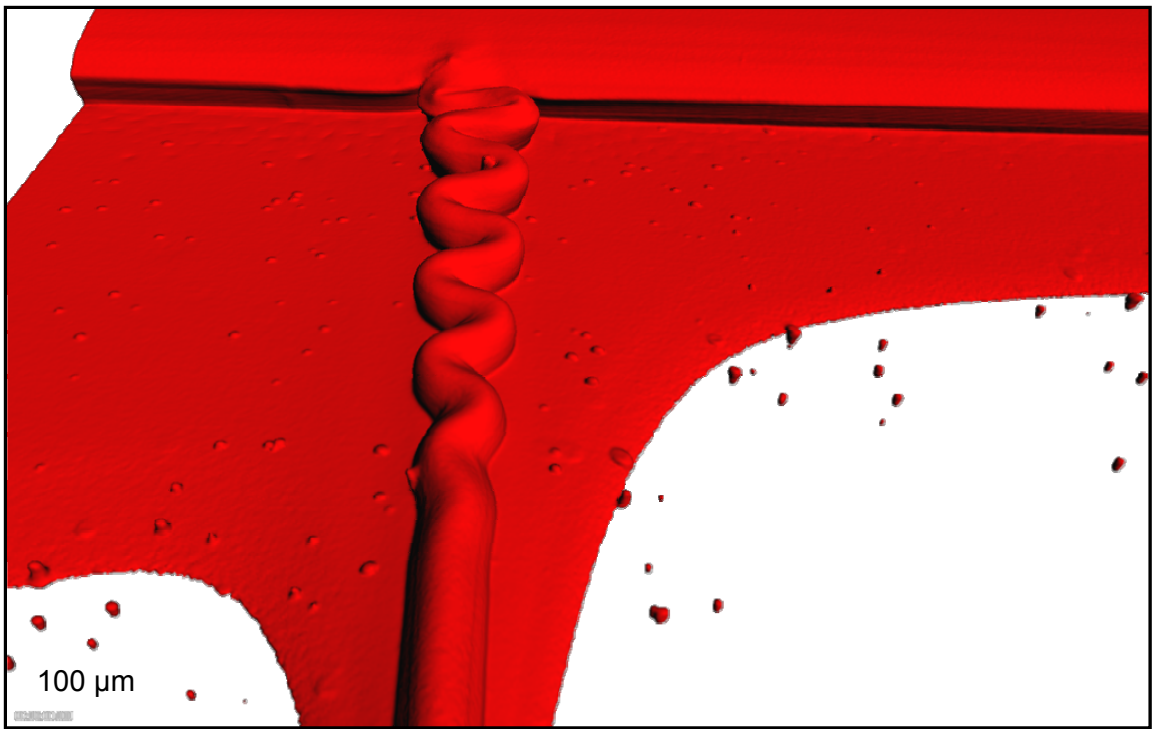

Figure 2-11: Polymer microstructure with surrounding polymer scum layer.

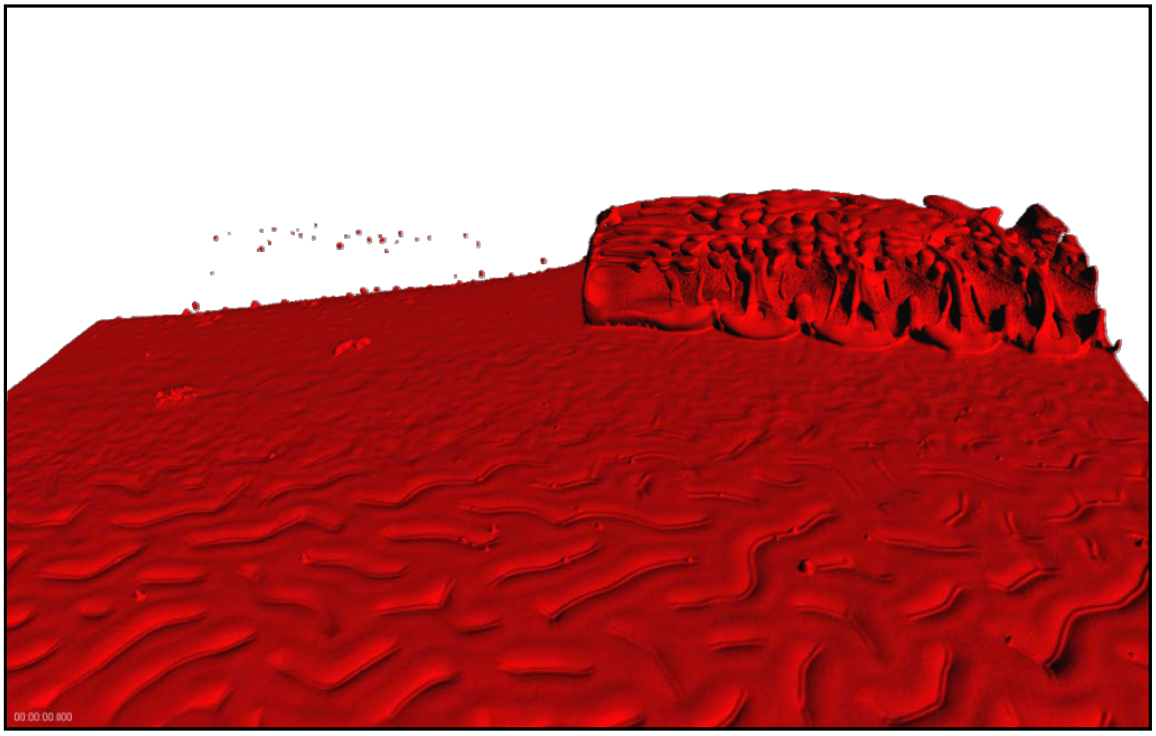

Figure 2-12: Deformed polymer pad (top-right corner) with surrounding scum layer exhibiting surface wrinkling.

2.5. Photopolymerization of Microgels

Microgels were created by MIMIC and used a prepolymer acetone/water (4:1) solution containing the following: 200 mg n-isopropylacrylamide monomer (97% Aldrich), 2 mg of 2-dimethoxy-2-phenylacetophenone (DMPA, Aldrich) as the photoinitiator, 1 mg polyfluor 570 fluorescent monomer (Methacryloxyethyl thiocarbonyl Rhodamine B) (Polysciences, Inc), and the crosslinker N,N'-Methylenebisacrylamide (varied from 0-40 mg, BIS, Chemzymes Ultra Pure).

Patterns of interest were cut out of the PDMS relief molds and placed pattern-down on the silanized surface. Because of PDMS's excellent adhesive properties, no further measure is required to bind them to the surface. As discussed in the section on MIMIC, applying these relief patterns to the surface creates a network of corridors. At the opening of these corridors, the pre-polymer solution is pooled and pressure created by capillary forces fills the corridors with the solution. Immediately after the pre-polymer solution has had time to fill the pattern, the assembly is photopolymerized using an uncollimated, 365 nm, 300 mW/cm^2 light source (EFOS Ultracure 100ss Plus, UV spot lamp, Mississauga, Ontario) for 5 minutes. Here it is imperative to start the polymerization as soon as possible, else solvent evaporation and subsequent crystallization (figure 2-13 and 2-14) are eminent[46]. The mixing of the pre-polymer solution from the prefabricated stocks as well as the MIMIC process described above, were all performed in a nitrogen environment.

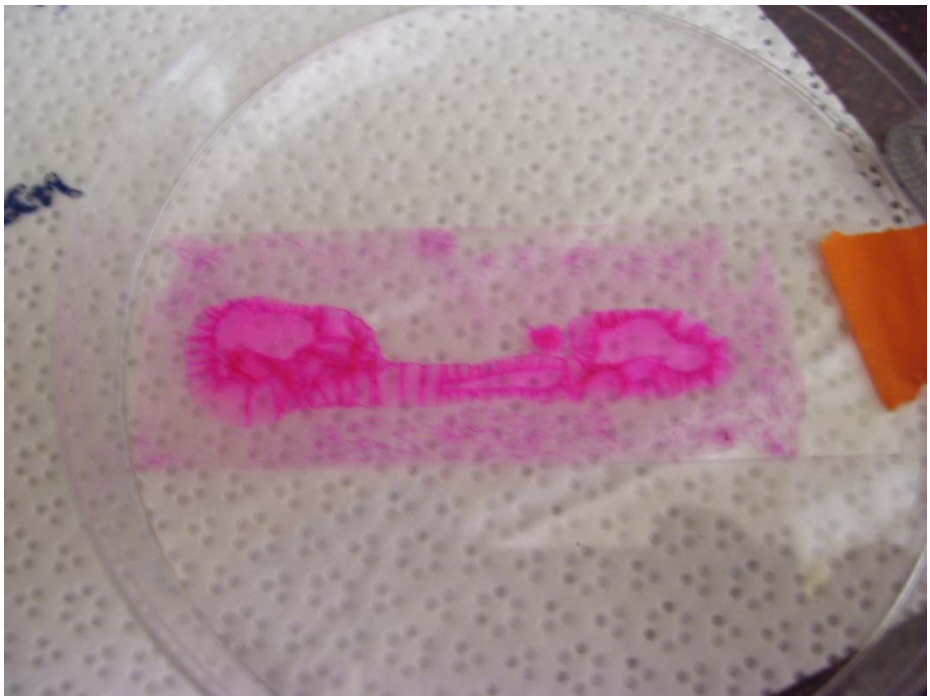

Figure 2-13: Slide with crystallized monomers (prepolymer solution) on it.

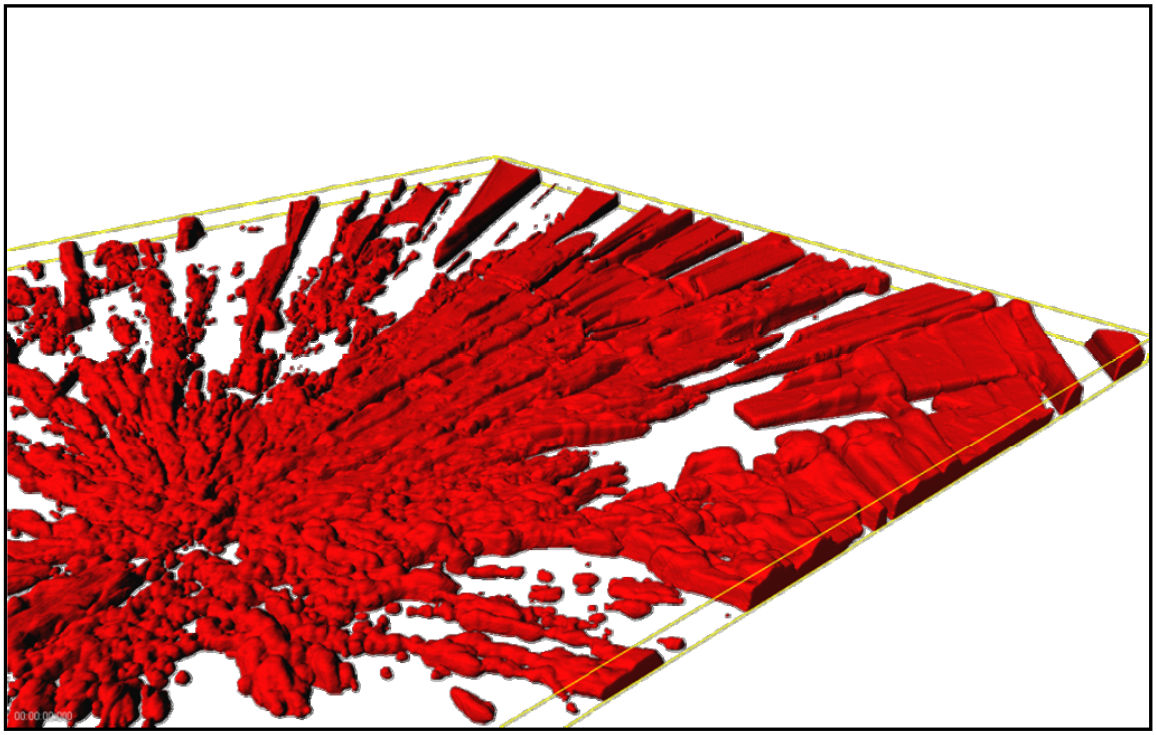

Figure 2-14: Confocal microscope image of crystallized monomer on the slide surface.

The formation of the hydrogel microstructures is performed through the photo-initiate free-radical polymerization of the acrylate end group in the NIPAAm monomers. In this reaction, DMPA is dissociated by the UV radiation, creating methyl radicals that then react with the carbon-carbon double bonds of the acrylate function group on the NIPAAm monomer. This reaction propagates between until it is terminated by the carbon-carbon double bond becoming oxygenated.

The silanated cover slide will also participate in this free radical reaction because of the availability of the vinyl groups (C=C) offered by the monolayer. This happens when the methacrylate radicals present in the NIPAAm monomer react with the vinyl groups and it forms covalent bonds which anchor the polymer to the monolayer[34].

While this process has been very useful in creating these microstructures, it is very inflexible in the variety of structures that can be made. This is due to the fact that the structures must be hydraulically connected. Thus isolated structures are an impossibility or must be created as hydraulically connected patterns and modified after the fact; a very tedious and altogether impractical endeavor. Also, this method, which relies on capillary forces, is only valid so long as the viscous forces at the corridor boundaries do not dominate; that is long patterns will experience too much viscous drag and will not fully fill with the pre-polymer mixture. However, interestingly enough, patterns that are short enough will fill even if the corridors have closed ends. It is thought that this occurs because small amounts of gas are able to diffuse into the PDMS elastomer[28]. Lastly, mechanically these PDMS relief patterns could be reused multiple times but due to the absorption of acetone and contamination, subsequent uses don’t yield desired results.

2.6. Fabrication of Fluid Cells

The fluid chamber was created by adhering individual glass cover slides (Corning, No. 1½, 25 mm2), each containing a single microstructure, to a plexiglass slide having dimensions of standard microscope slides. The plexiglass overlay was prefabricated with holes, such that each microstructure would be encased in the plexiglass (forming a fluid well). This design is shown in figure 2-15 and 2-16. The design presented in figures 2-15 and 2-16 is the most recent design but the evolution of the fluid cell design can be seen in figure 2-17. Nail polish was used to adhere the plexiglass to the glass substrate. From here DI water can easily be added or removed from this minimalistic design that easily accommodates the inverted confocal microscope.

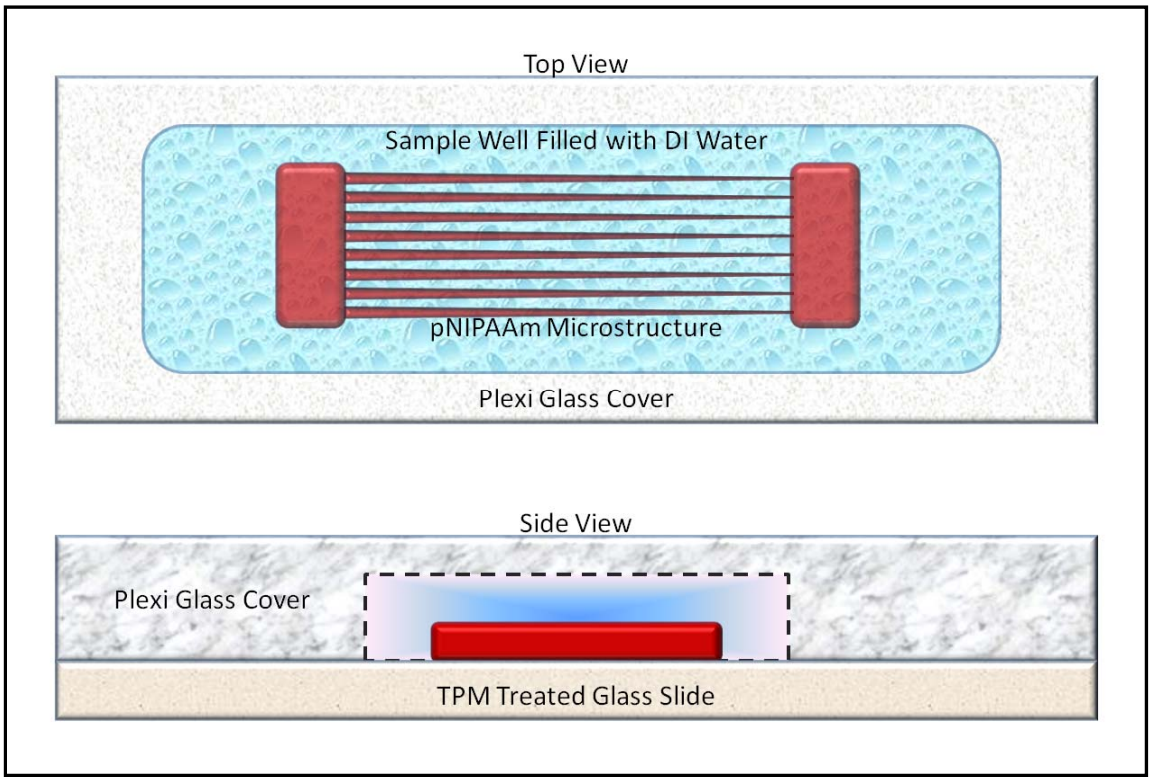

Figure 2-15: Top and side view of assembled fluid cell.

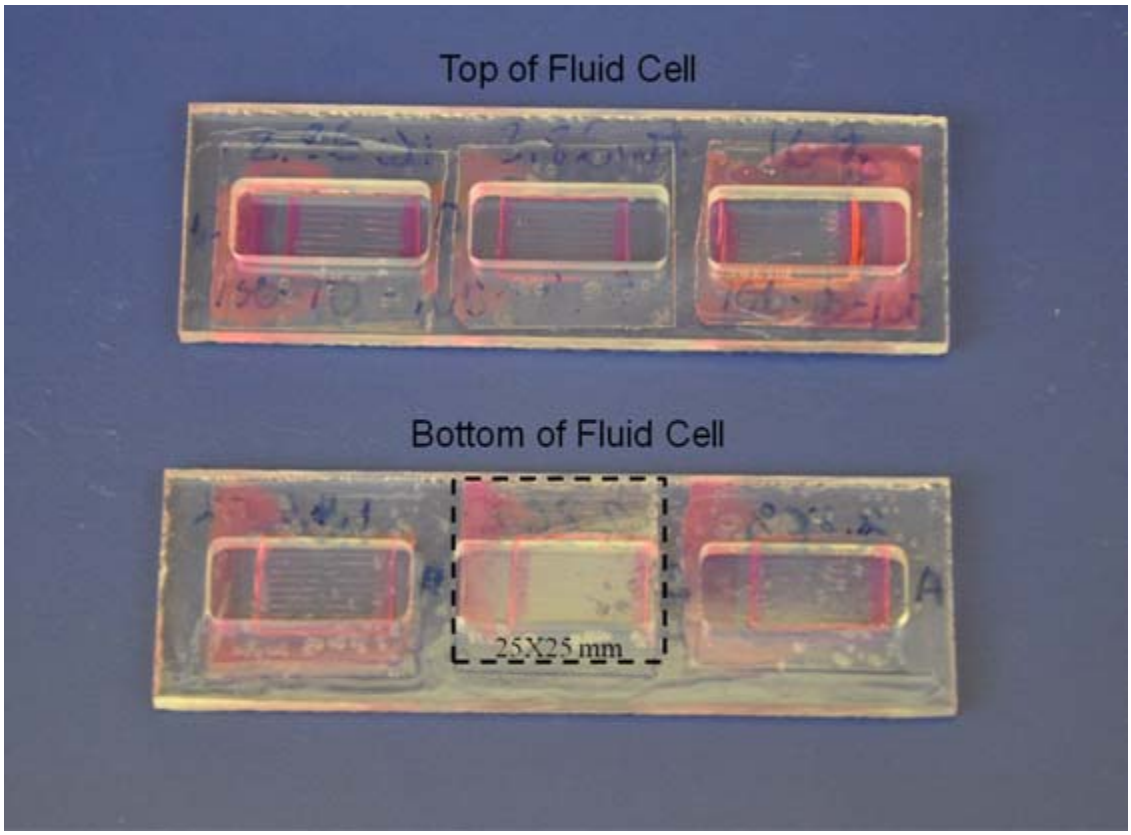

Figure 2-16: Top and bottom view of fluid cell with sample slide adhered.

Figure 2-17: Chronicle evolution of fluid cell design. First design (left) was an enclosed design that used a plexiglass cover with ports. The latter two (to the right) were open top designs with open tops.

2.7. Remarks

All pattern PNIPAAm microstructures that are created with this method seem to display a decrease in structure height at the midway point between hydraulic pads. It is not certain whether this is caused by bowing of the PDMS relief mold or if the tops of the structures in that part of the pattern are being torn off. The latter is not supported by closer examination of the PDMS stamp after polymerization. Further investigation is needed.

CHAPTER THREE: CHARACTERIZATION OF EXTENT OF SWELLING AND CROSSLINK DENSITY

3.1. Introduction

The most important characteristic of thermo-responsive gels is their ability to readily swell and deswell. This makes absorption capacity the most crucial property of these gels. The primary variables that control this property are the ion content of the polymer matrix, the crosslink density and the solvent interaction parameter (χ_1) [47]. Because PNIPAAm is a nonionic polymer and the solvent used is constant, the crosslink density is the remaining variable which must be determined experimentally. Of the available experiments for determining crosslink density (stretching, compressing, indenting, etc…), equilibrium swelling was chosen to characterize this parameter. Knowledge of the swelling limits of the hydro gel can then be combined with equilibrium swelling theory and Flory-Huggins mixing theory to determine the crosslink concentration [47].

3.2. Characterization of Extent of Swelling in Bulk Gels

In order to get a general understanding of the swelling dependence on crosslink density, marcoscale swelling test were conducted for 15 different samples over a spread of 0-20 wt% BIS (weight ratio BIS/NIPAAm ~= wt% BIS). This was accomplished by fabricated 15 (1ml) microgel samples at different crosslink concentration and placing them in water baths below and then above the LCST and measuring the changes in

mass. With the given density of water (0.997 g/cm^3 and 0.992 g/cm^3) at these operating temperatures (21.5°C and 40°C, on average), the volume change and hence the degree of swelling can be calculated.

3.2.1. Experimental Procedure

PNIPAAm gels were fabrication in 12 x 75 mm disposable culture tubes in a nitrogen environment at room temperature and pressure. The procedure is as follows:

3.2.1.1. Preparing the Stock Solutions

The desired prepolymer solution contains 200mg of monomer N-isopropylacrylamide, 2 mg of photoinitiator 2,2-dimethoxy-2-phenylacetophenone (DMPA), 0.5 mg of fluorescents monomer polyfluor 570 (Methacryloxyethyl thiocarbonyl Rhodamine B), and 5 mg of crosslinker N,N'-methylenebisacrylammide (MBS) all in a 1 ml portion of solvent. In order to make multiple prepolymer solutions with accuracy, weighing out small quantities was avoided and instead stock solutions of all of the constituents were created. To make for easy variability of the MBS, the mass of each of the solute needed in the final solution was added to 1 ml of acetone and then the concentrations of all four were quadrupled to yield the following in table 3-1.

Table 3-1: Initial prepolymer solutions recipe.

Solute	mg. of solute	Conc. of Stocks (mg/ml)	4 x Conc.	wt% solutes
NIPAAm	200	200	800	96.3855%
DMPA	2	2	8	0.9639%
Rhodamine	0.5	0.5	2	0.2410%
MBS	5	5	20	2.4096%

For this base recipe, which has been used in previous work by DuPont et al[17], the current weight ratio of BIS to NIPAAm is 2.5%. It is desire to have a maximum weight ratio of 20% and a minimum of 0%. At 20 wt%, the concentration of the BIS solution climbs to 160 mg/ml. To achieve this, a battery of 15 samples were created to cover this span by altering the concentration of the BIS stock with acetone to maintain and equal ¼ volume contribution to the prepolymer mix, as shown by table 3-2.

Table 3-2: BIS dilution chart.

Solution	MBS (mg)	wt% MBS/NIPAAm	Actetone (µl)	BIS stock (µl)
1	0	0.00%	250.00	0.00
2	11.429	1.43%	246.43	3.57
3	22.857	2.86%	239.39	10.61
4	34.286	4.29%	229.13	20.87
5	45.714	5.71%	216.04	33.96
6	57.143	7.14%	200.60	49.40
7	68.571	8.57%	183.41	66.59
8	80.000	10.00%	165.07	84.93
9	91.429	11.43%	146.20	103.80
10	102.857	12.86%	127.41	122.59
11	114.286	14.29%	109.21	140.79
12	125.714	15.71%	92.04	157.96
13	137.143	17.14%	76.27	173.73
14	148.571	18.57%	62.10	187.90
15	160.000	20.00%	0.00	250.00

Unfortunately, BIS has a solubility of ~8 mg/ml in pure acetone. Trying to stay as close to the original solvent as possible, so that data collect on microgel from previous work would still be prudent, a solubility test with acetone/water mixtures conducted with BIS, as shown in figure 3-1.

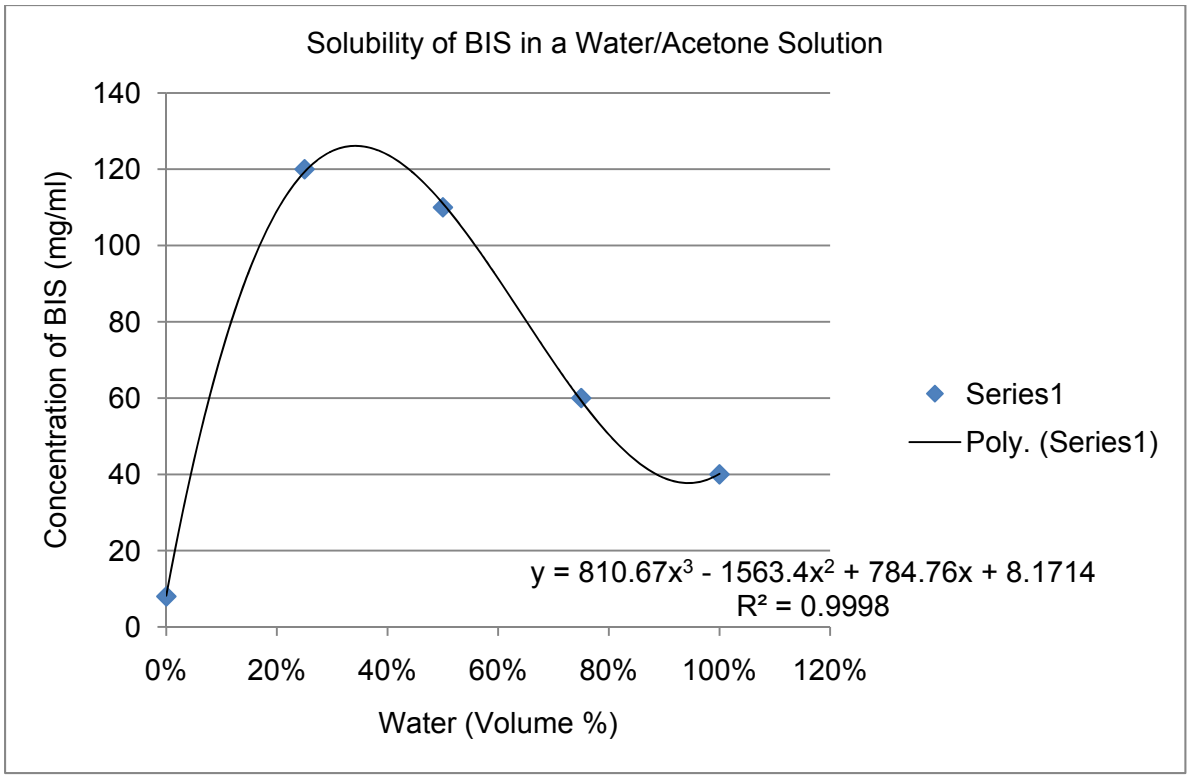

Figure 3-1: Solubility plot of BIS concentration verses water to acetone volume ratios

Based on this, a stock of BIS was made with a 25/75% water/acetone mixture and it was found to form a suspension with a low settling rate. In lieu of switching to a different solvent this was used. Also, to maintain a 25/75% solvent mixture, the DMPA stock was quadrupled again (now 8x the original) and added as 1 part DMPA stock to 3 parts DI water for the DMPA's contribution to the prepolymer solution. The final recipe and dilution table now read as follows in tables 3-3 & 3-4.

Table 3-3: Revised prepolymer recipe for equal volume contribution.

Solute	mg of solute	Conc. of Stocks (mg/ml)	4 x Conc.	wt% solutes
NIPAAm	200	200	800	96.3855%
DMPA	2	2	16	0.9639%
Rhodamine	0.5	0.5	2	0.2410%
MBS	40	40	160	19.2771%

Table 3-4: Dilution chart for BIS.

Solution	MBS (mg)	wt% MBS/NiPAAm	Actetone (µl)	Stock (µl)
1	0	0.00%	250.00	0.00
2	11.429	1.43%	246.43	3.57
3	22.857	2.86%	239.39	10.61
4	34.286	4.29%	229.13	20.87
5	45.714	5.71%	216.04	33.96
6	57.143	7.14%	200.60	49.40
7	68.571	8.57%	183.41	66.59
8	80.000	10.00%	165.07	84.93
9	91.429	11.43%	146.20	103.80
10	102.857	12.86%	127.41	122.59
11	114.286	14.29%	109.21	140.79
12	125.714	15.71%	92.04	157.96
13	137.143	17.14%	76.27	173.73
14	148.571	18.57%	62.10	187.90
15	160.000	20.00%	0.00	250.00

The stock solutions for NIPAAm were made with 5 ml of acetone for the stock, while 20 ml was used for the remaining solutes.

The first two batches of samples and swell test were conducted using this recipe and method until it was discovered that an error had been made; the solvent added to the BIS stock was pure acetone instead of a 25/75 volume ratio of water and acetone. This would have thrown off the whole ratio of the solvent which was to be maintained at

25/75 to preserve optimal solvating conditions. The dilution table was reworked, as shown in table 3-5, and the next two batches of samples and swell test were conducted with this correction.

Table 3-5: Revised dilution chart for BIS.

Solution	mg MBS	wt% MBS/NiPAAm	25/75% Water/Actetone	ul Stock
1	0	0.00%	250.00	0.00
2	11.429	1.43%	246.43	3.57
3	22.857	2.86%	239.39	10.61
4	34.286	4.29%	229.13	20.87
5	45.714	5.71%	216.04	33.96
6	57.143	7.14%	200.60	49.40
7	68.571	8.57%	183.41	66.59
8	80.000	10.00%	165.07	84.93
9	91.429	11.43%	146.20	103.80
10	102.857	12.86%	127.41	122.59
11	114.286	14.29%	109.21	140.79
12	125.714	15.71%	92.04	157.96
13	137.143	17.14%	76.27	173.73
14	148.571	18.57%	62.10	187.90
15	160.000	20.00%	0.00	250.00

3.2.1.2. Sample Preparation

The 15 samples were prepared five at a time with the same procedure for each of the 4 total batches. Each batch was placed in a test tube rack outside of the nitrogen tent and was dispensed its prescribed BIS concentration and the 3 parts DI water that was to be added to the DMPA's aliquot (187.5 µl). In order to maintain a consistent suspension of BIS, the BIS stock solution was first agitated on a Vortex Genie 2 (Model G-560) for 10 minutes and then place on a stir plate to maintain agitation for the duration of the sample preparation. The remaining ingredients were added in the glove bag under a positive pressure of nitrogen. After all of the ingredients were added the culture tubes

were all stirred well to insure proper mixing of the prepolymer solution. At this point the samples were irradiated with a UV spot lamp for 15 minutes under constant agitation. Once polymerized, all samples were removed from the glove bad and either shaken from their culture tubes or the tubes were gently fractured and the sample were removed. All samples were then placed in 60 ml graduated glass bottles and labeled with their respective BIS concentration.

3.2.1.3. Experimental Setup and Data Collection

Once all samples were finished, 20 ml of DI water at 21.5 °C (on average) was added to each specimen container and then they were sealed. Mass measurements were recorded by removing the samples and drying off any superficial water before recording a data point. Data of all of the samples were taken every 30 minutes during the initial 3 hours of swelling due to the steep rate of change. After each recorded mass, 20 ml of fresh DI water was added to replace the used water. This was done do limit the affects of excess solvent or unreacted monomer. All subsequent readings occurred only as often as needed.

After 120 hours of data collection had past, all sample's DI water was replaced by heated DI water at approximately 40 °C and then they were placed in 1000 ml beakers containing 200 ml of DI water also at approximately 40 °C. The increments at which data was nearly identical to regiment followed for the swelling portion of the experiment. Deswelling data was also taken for the duration of 120 hours.

After deswelling, all samples were placed in labeled Pyrex Petri dishes and heated in an Isotemp® vacuum oven (Model 280A) furnace at 75 °C under a constant 2.92 mmHg of vacuum for 24 hours. Samples were then removed and their dry mass was recorded. All samples were stored in their dry state.

3.2.2. Remarks and Results

To calculate the crosslink density from extent of swelling data, one only needs the volume of the original sample, the most swollen state and the dry state but additional data was collected over the duration of the swelling so that a qualitative assessment of the data may be made. The swelling and deswelling data for all 4 batches is listed in figures 3-2 through 3-17. It is important to note that samples 1 and 2 were created with the acetone rich recipe. Sample 3 and 4 were made with the recipe that keeps a constant 25/75 volume % of water and acetone, respectively.

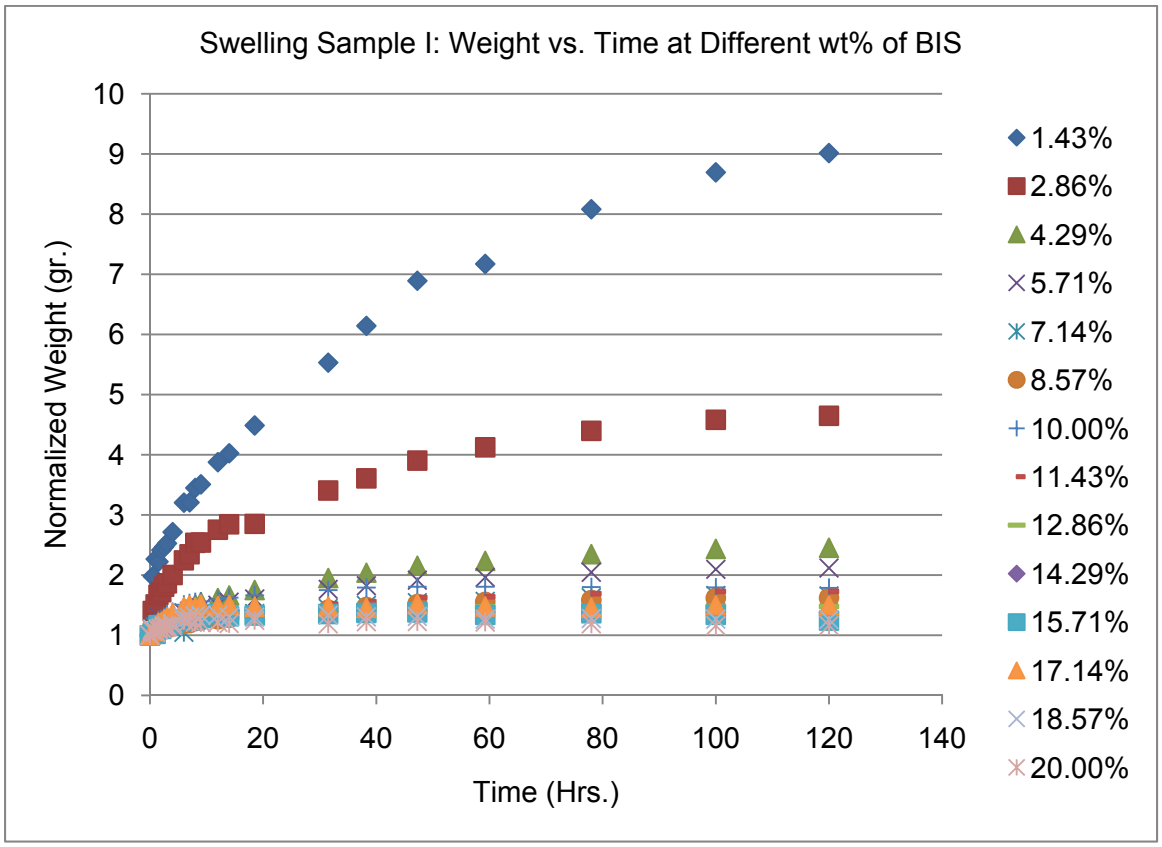

Figure 3-2: Swelling of 1ml PNIPAAm samples with variable BIS (crosslinker) concentrations.

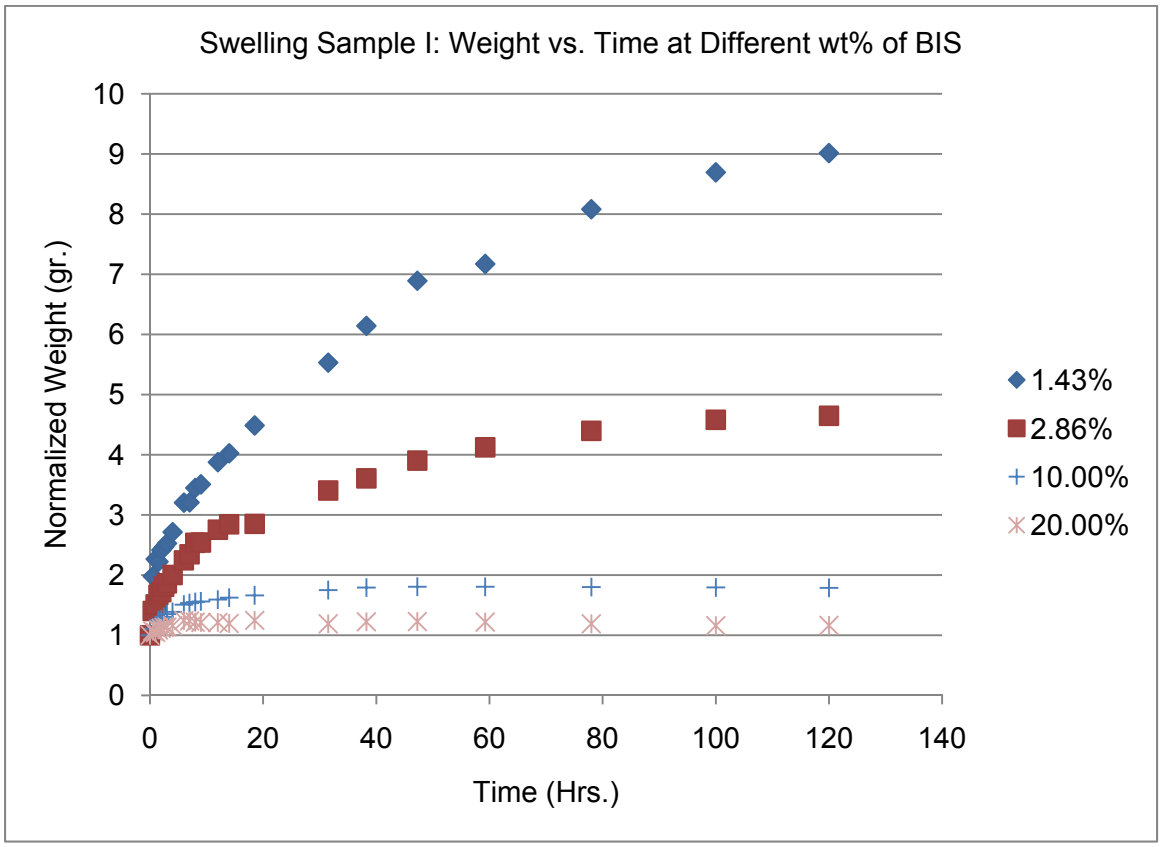

Figure 3-3: Swelling of 1ml PNIPAAm samples with only four select weight ratios of BIS/NIPAAm shown.

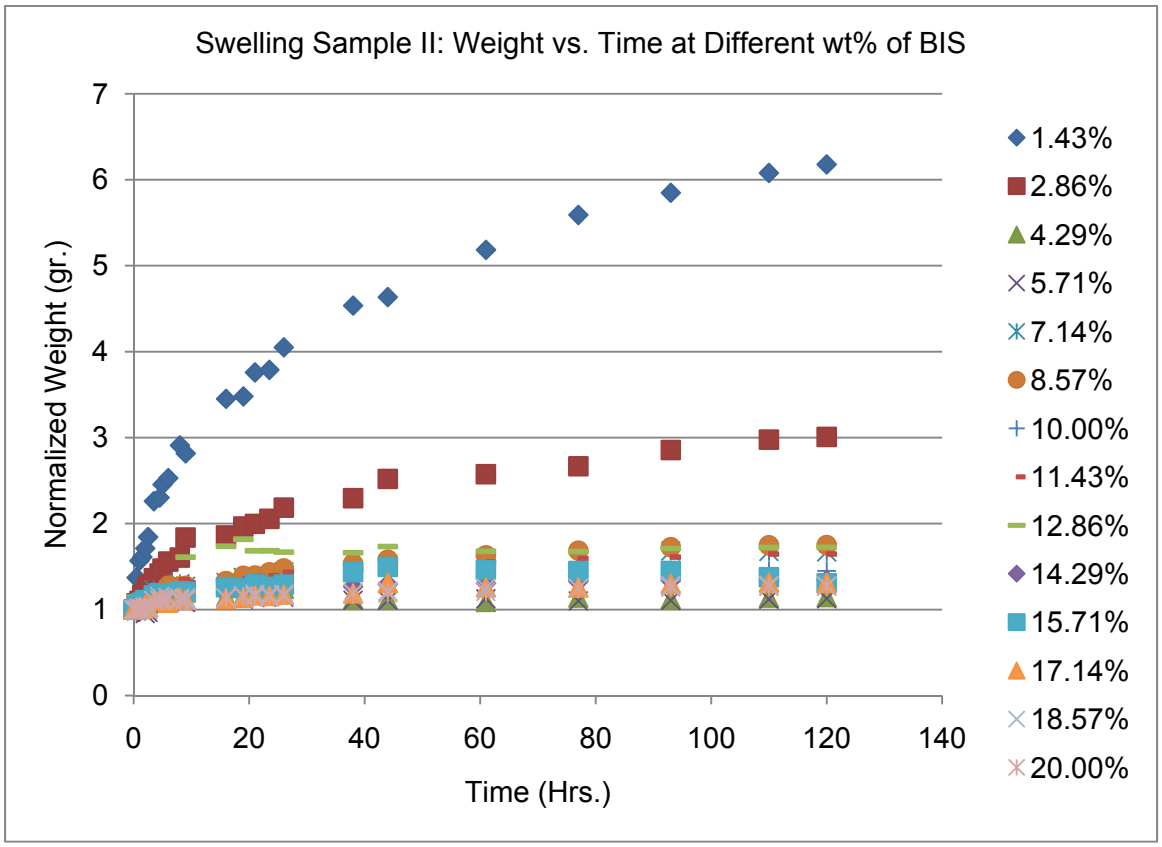

Figure 3-4: Swelling of 1ml PNIPAAm samples with variable BIS (crosslinker) concentrations.

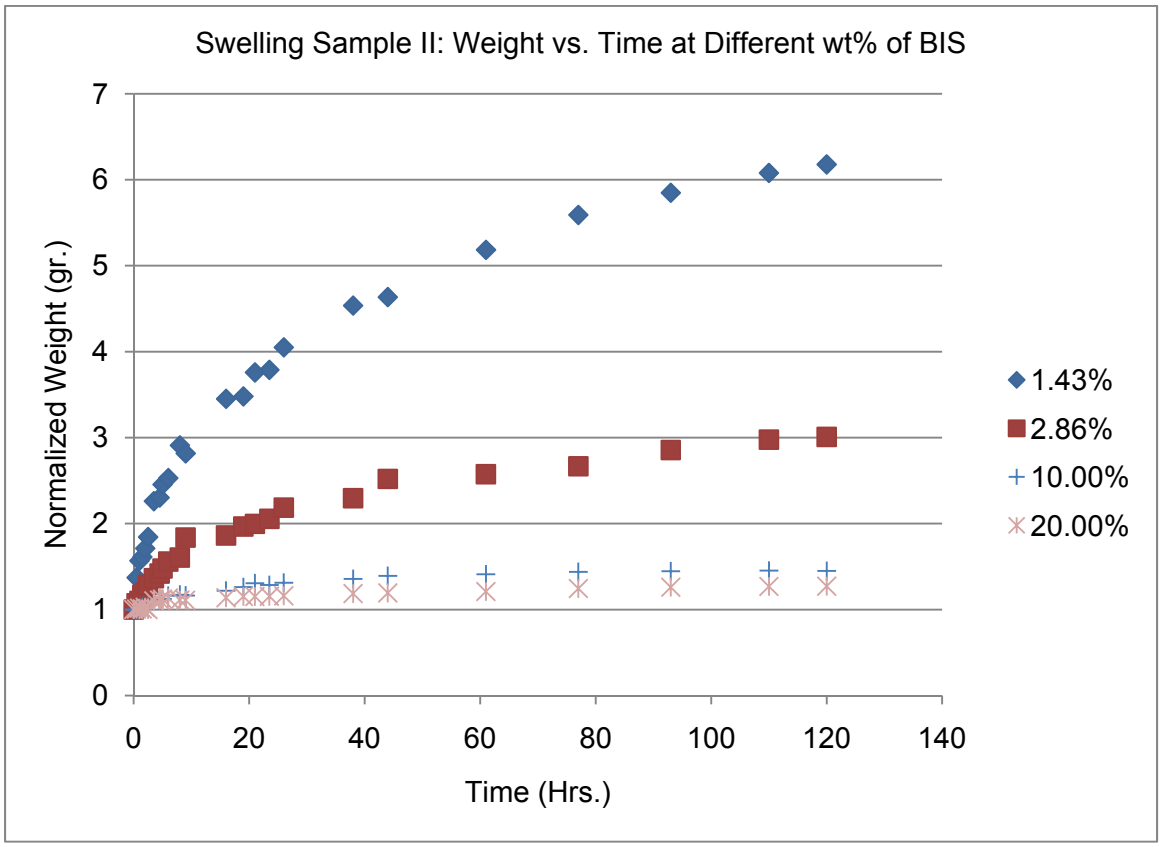

Figure 3-5: Swelling of 1ml PNIPAAm samples with only four select weight ratios of BIS/NIPAAm shown.

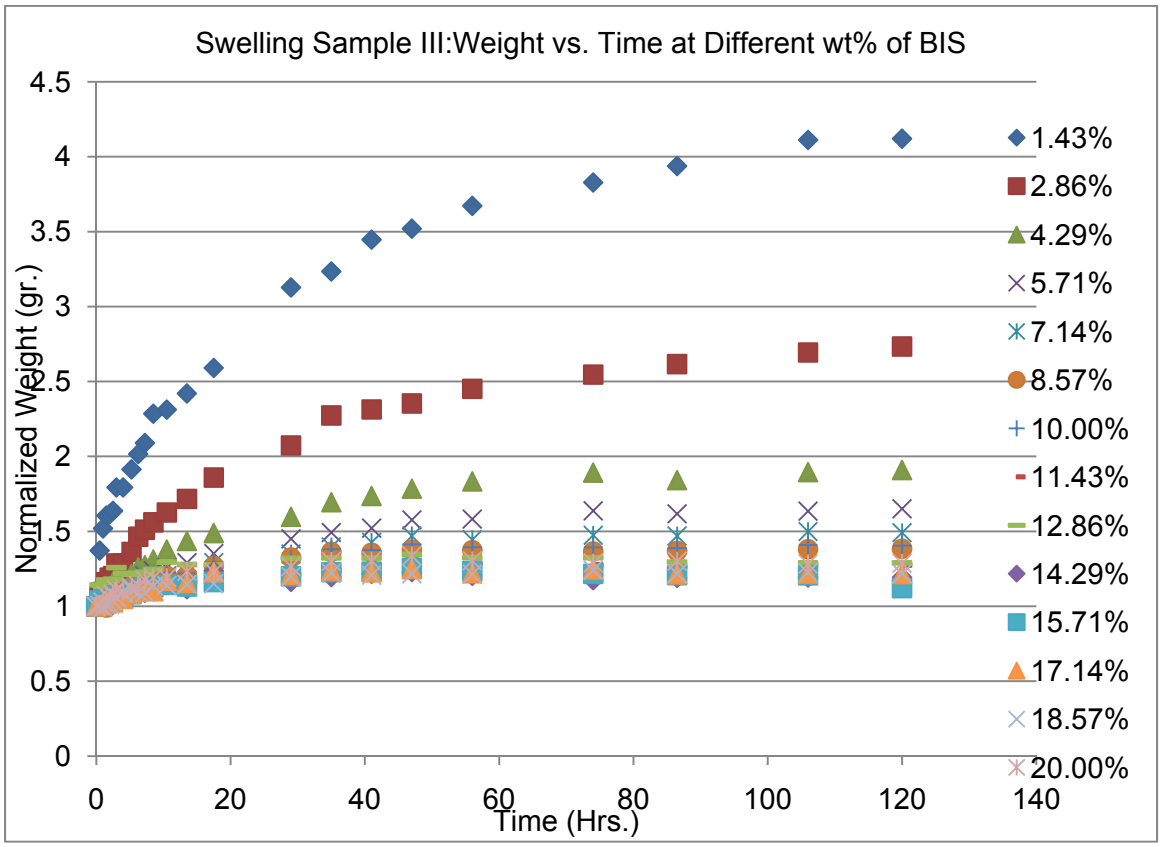

Figure 3-6: Swelling of 1ml PNIPAAm samples with variable BIS (crosslinker) concentrations.

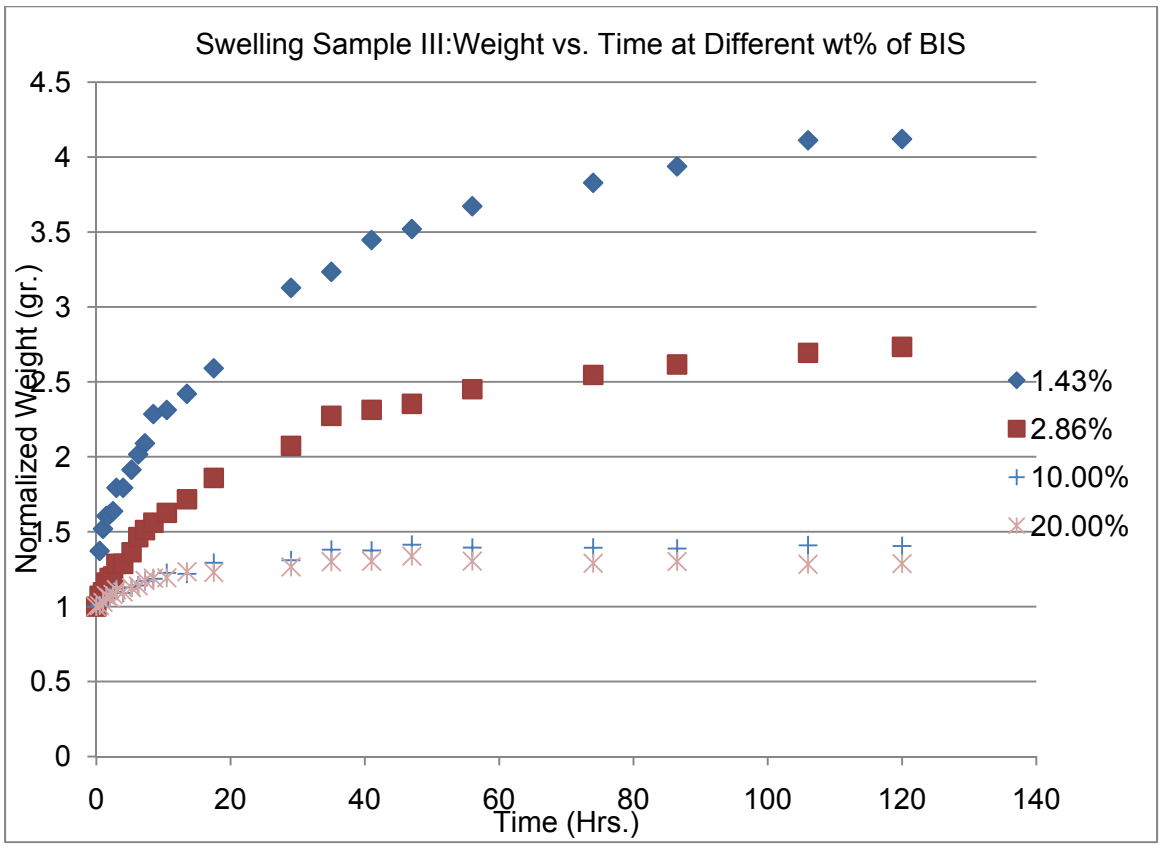

Figure 3-7: Swelling of 1ml PNIPAAm samples with only four select weight ratios of BIS/NIPAAm shown.

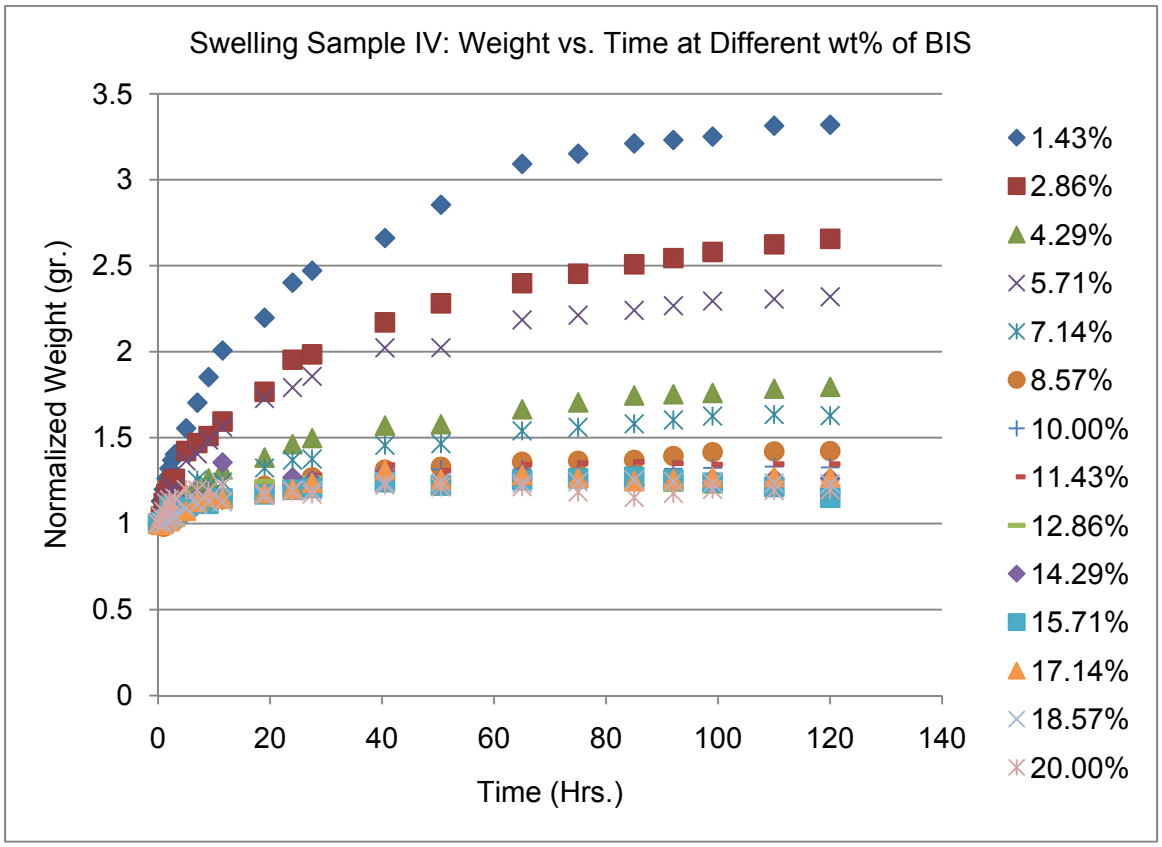

Figure 3-8: Swelling of 1ml PNIPAAm samples with variable BIS (crosslinker) concentrations.

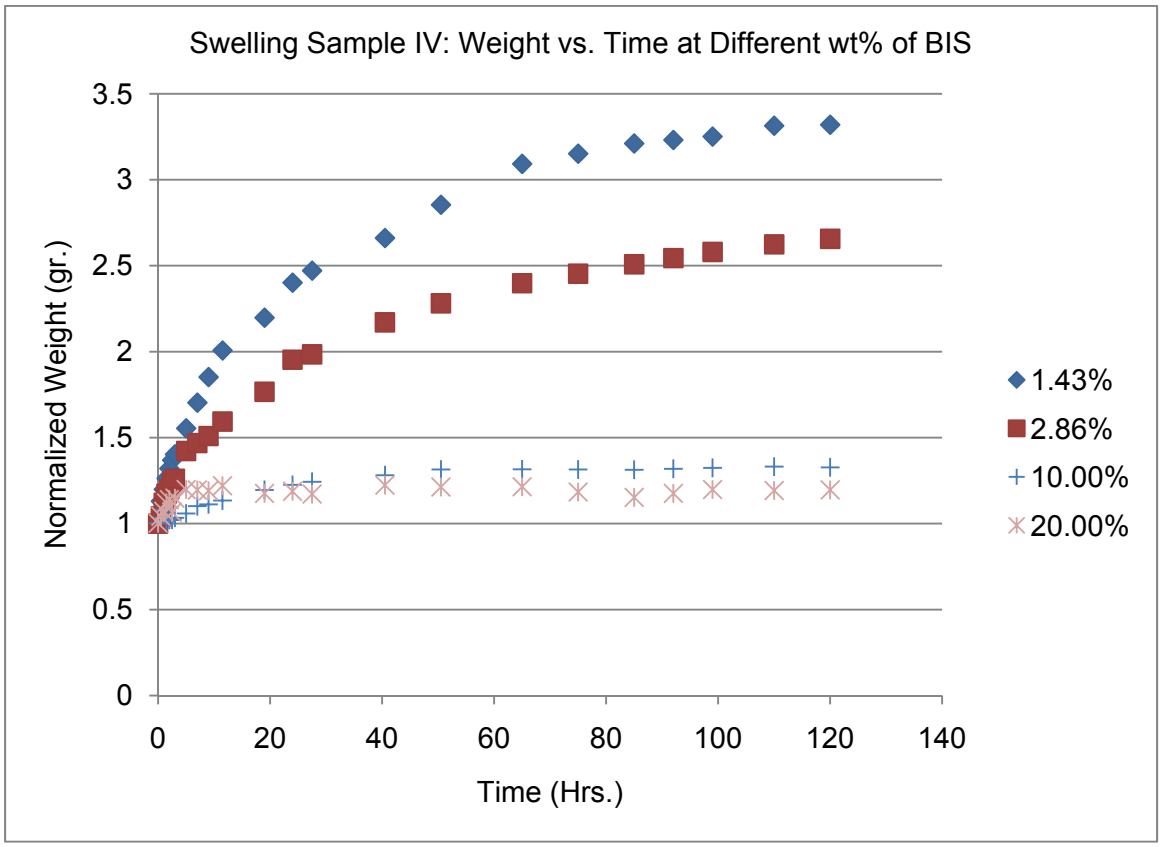

Figure 3-9: Swelling of 1ml PNIPAAm samples with only four select weight ratios of BIS/NIPAAm shown.

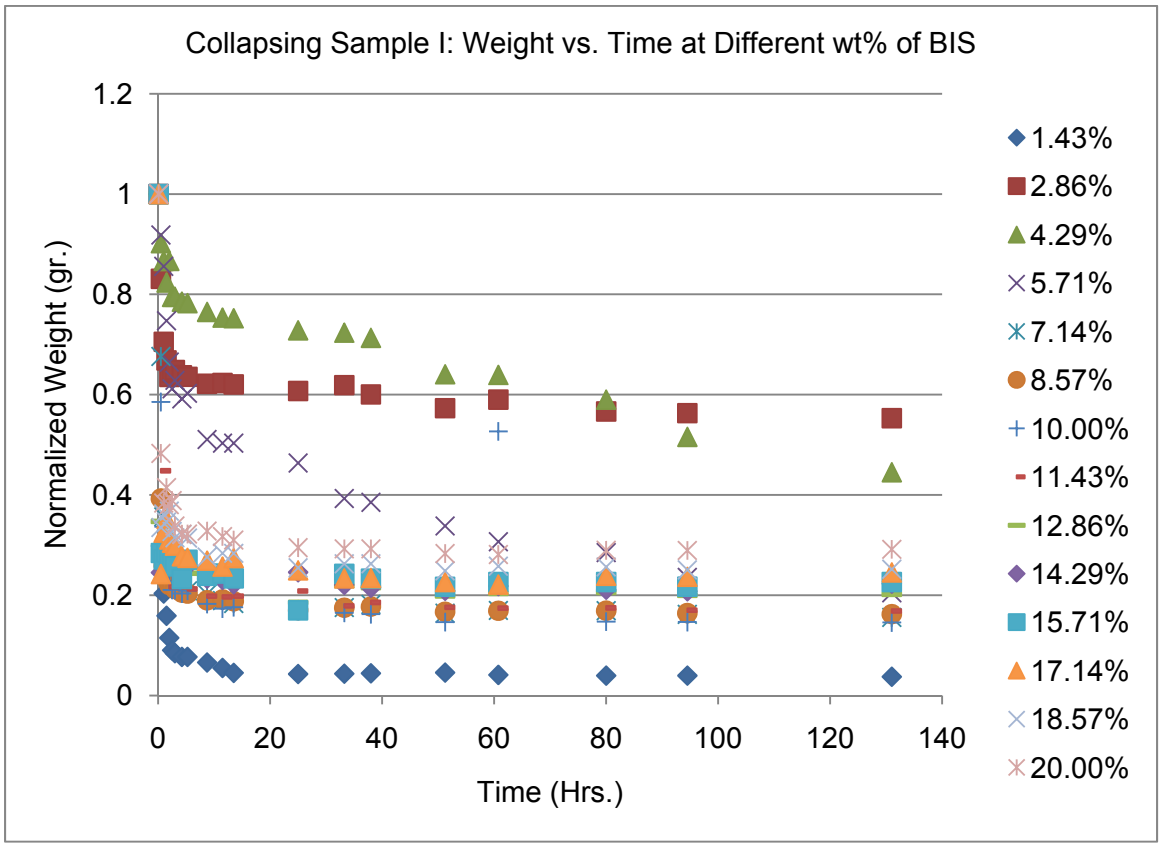

Figure 3-10: Deswelling of 1ml PNIPAAm samples with variable BIS (crosslinker) concentrations.

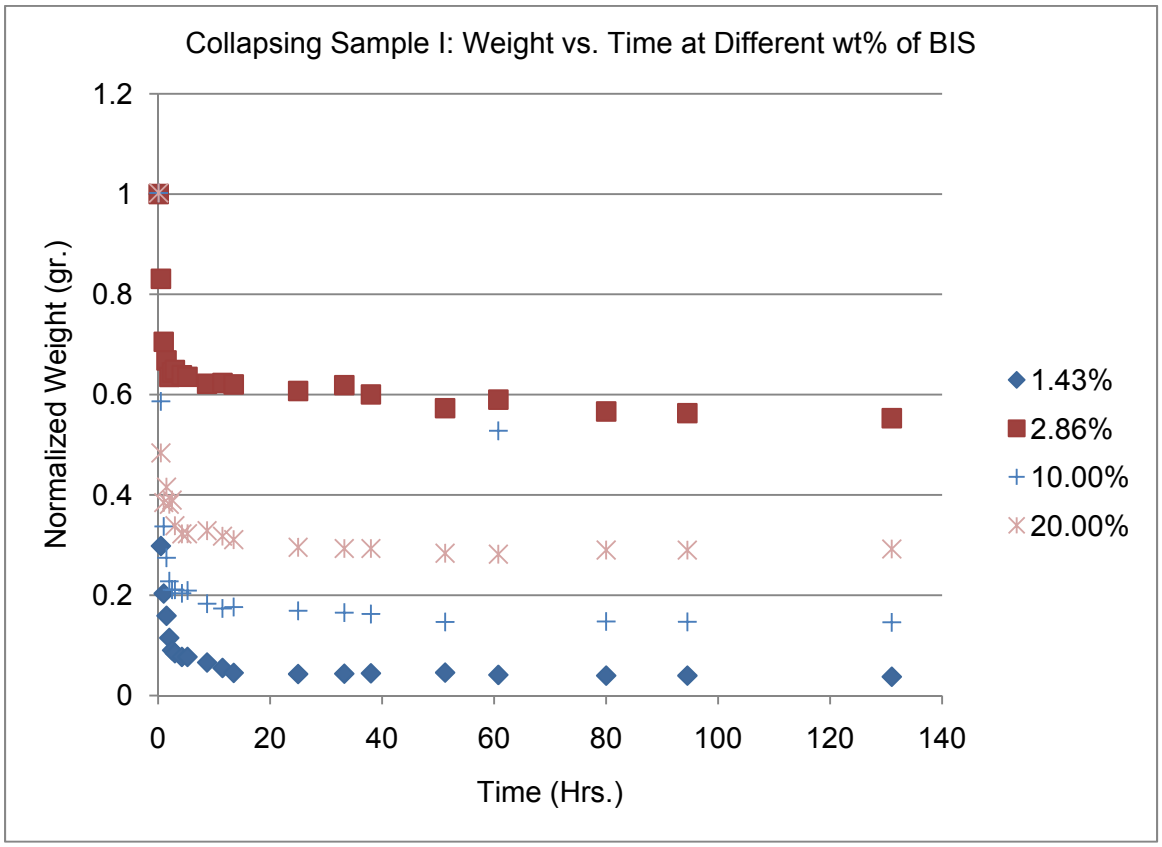

Figure 3-1: Deswelling of 1ml PNIPAAm samples with only four select weight ratios of BIS/NIPAAm shown.

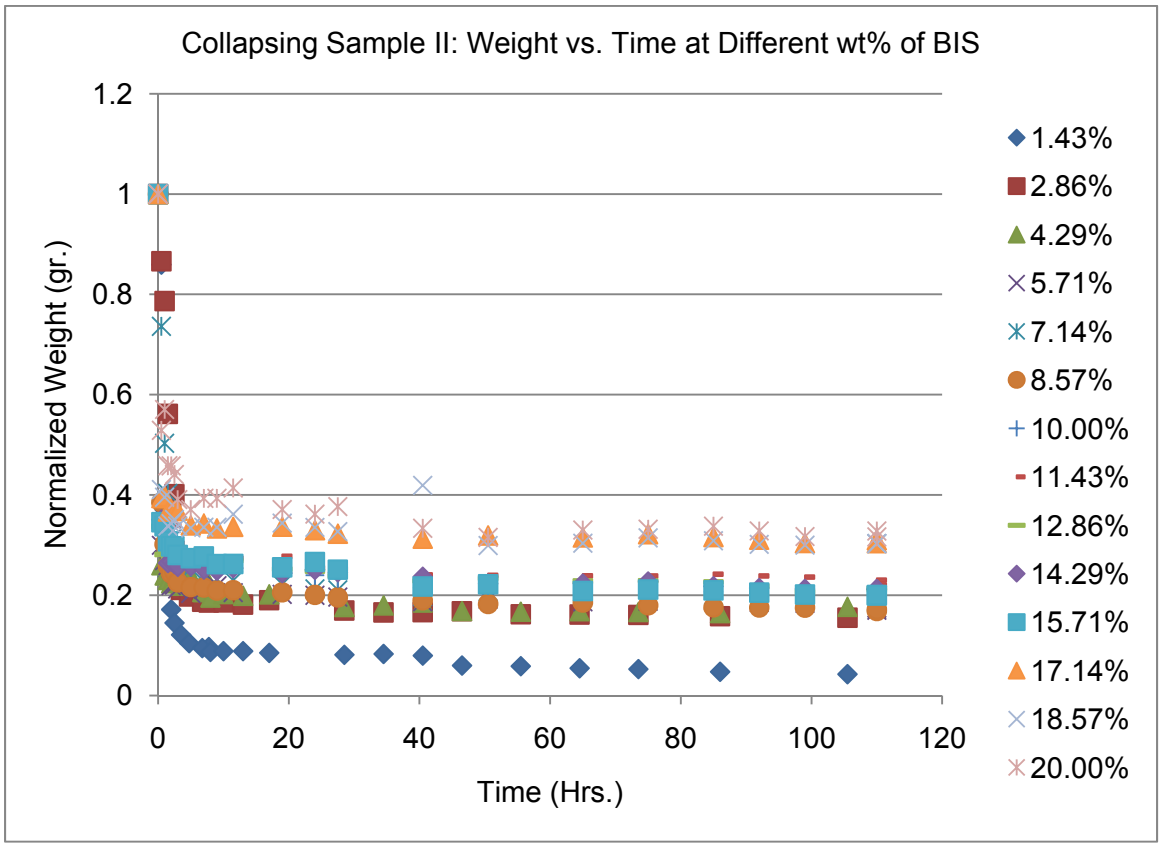

Figure 3-2: Deswelling of 1ml PNIPAAm samples with variable BIS (crosslinker) concentrations.

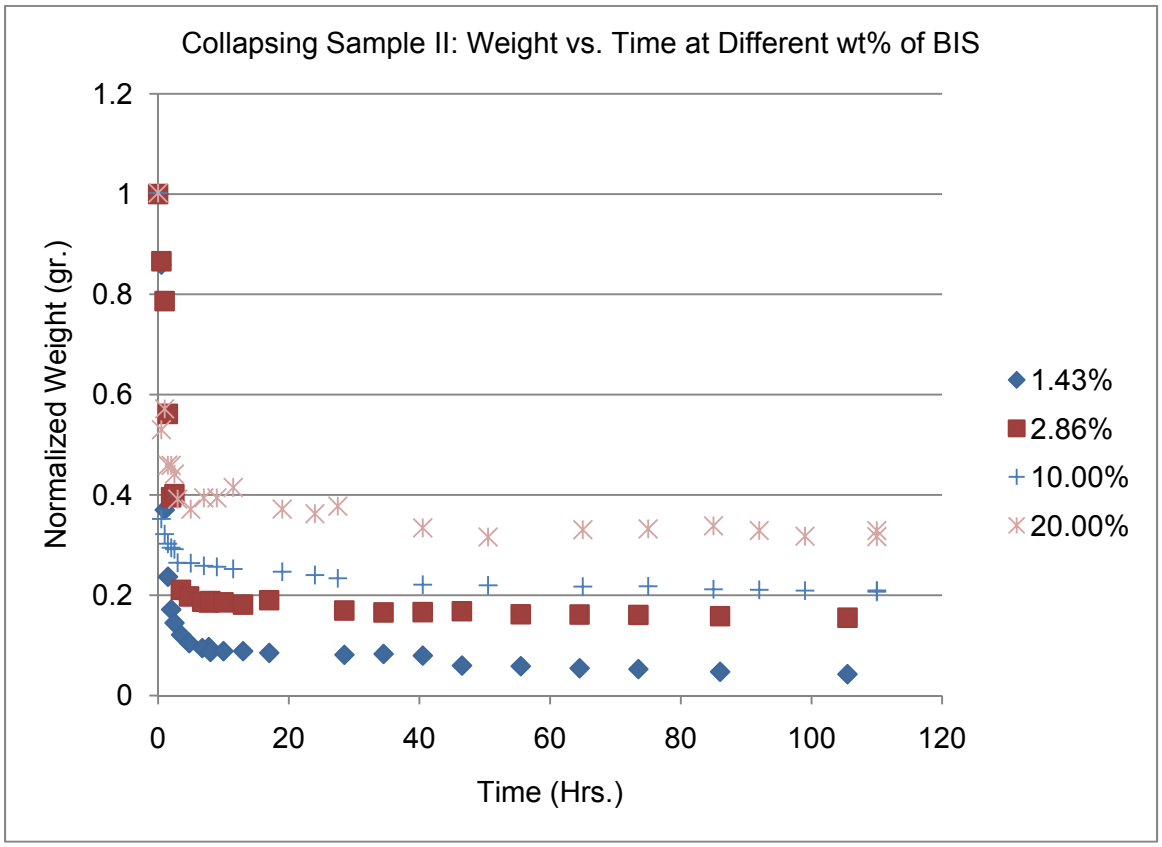

Figure 3-3: Deswelling of 1ml PNIPAAm samples with only four select weight ratios of BIS/NIPAAm shown.

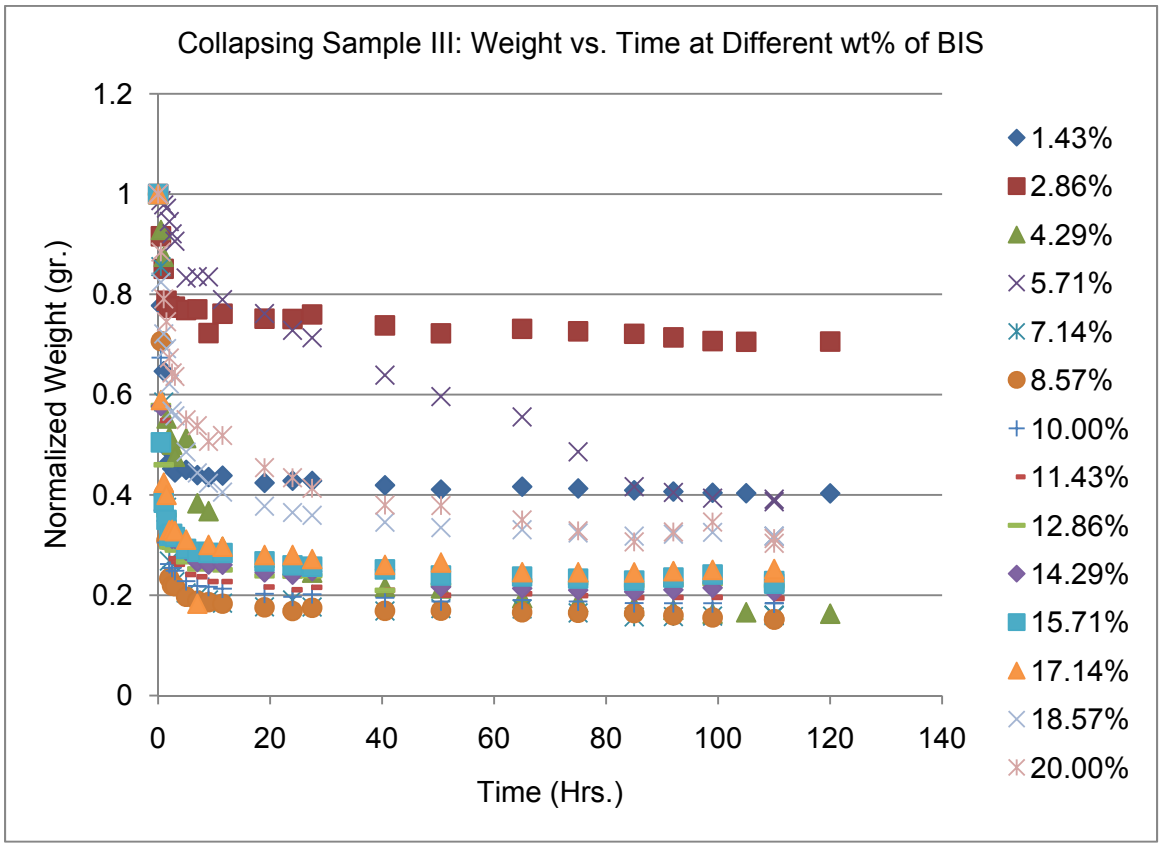

Figure 3-4: Deswelling of 1ml PNIPAAm samples with variable BIS (crosslinker) concentrations.

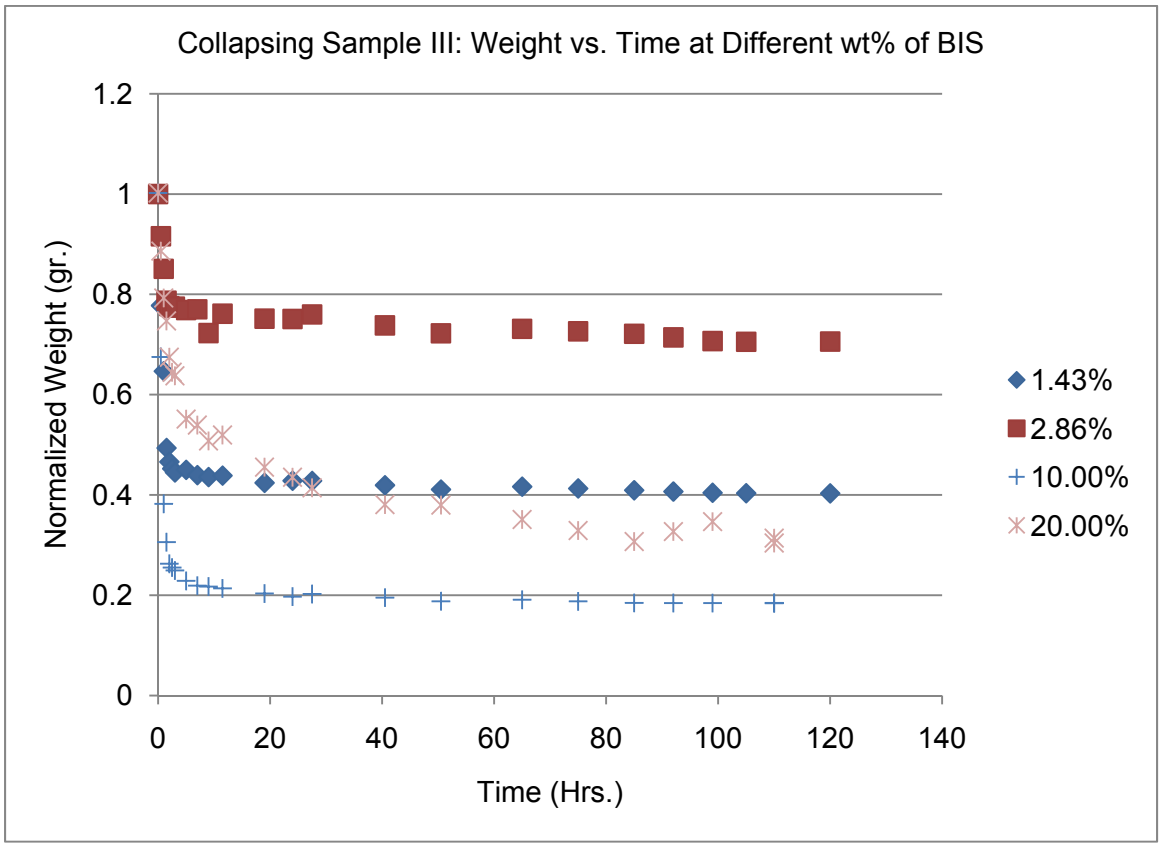

Figure 3-5: Deswelling of 1ml PNIPAAm samples with only four select weight ratios of BIS/NIPAAm shown.

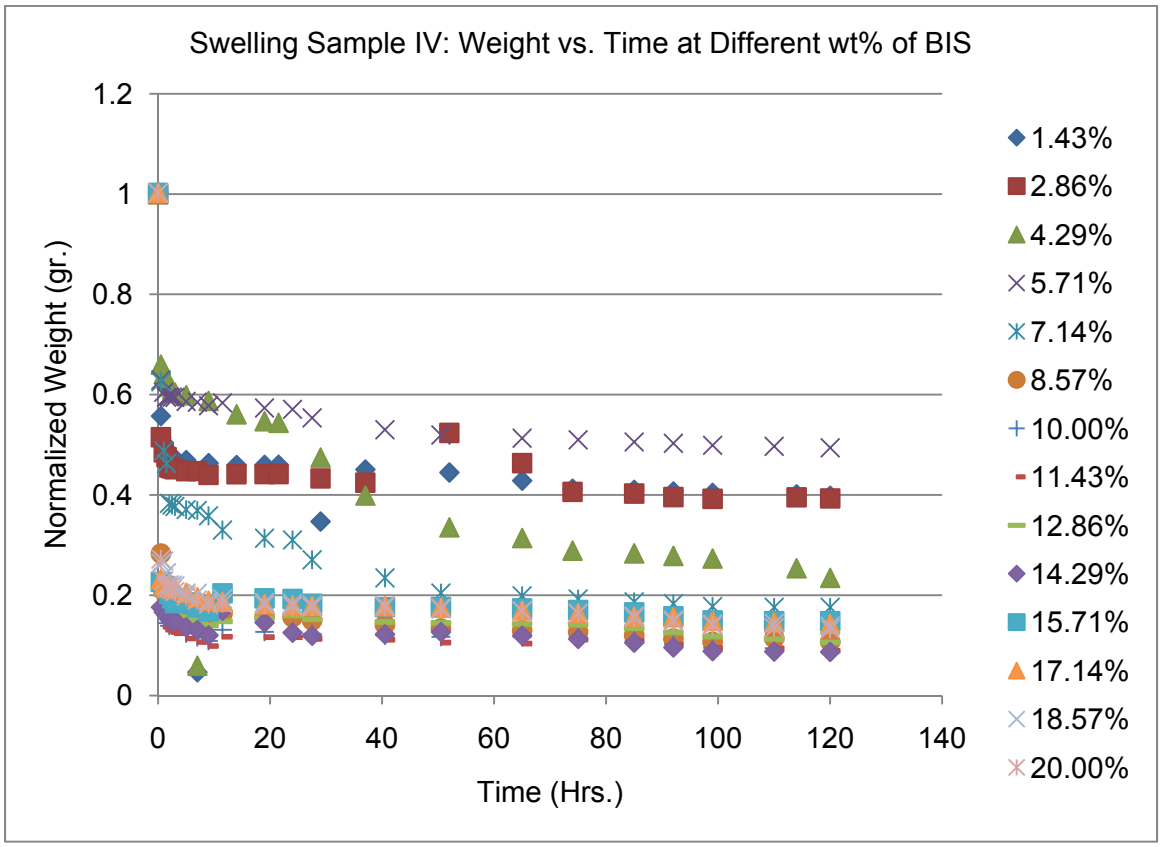

Figure 3-66: Deswelling of 1ml PNIPAAm samples with variable BIS (crosslinker) concentrations.

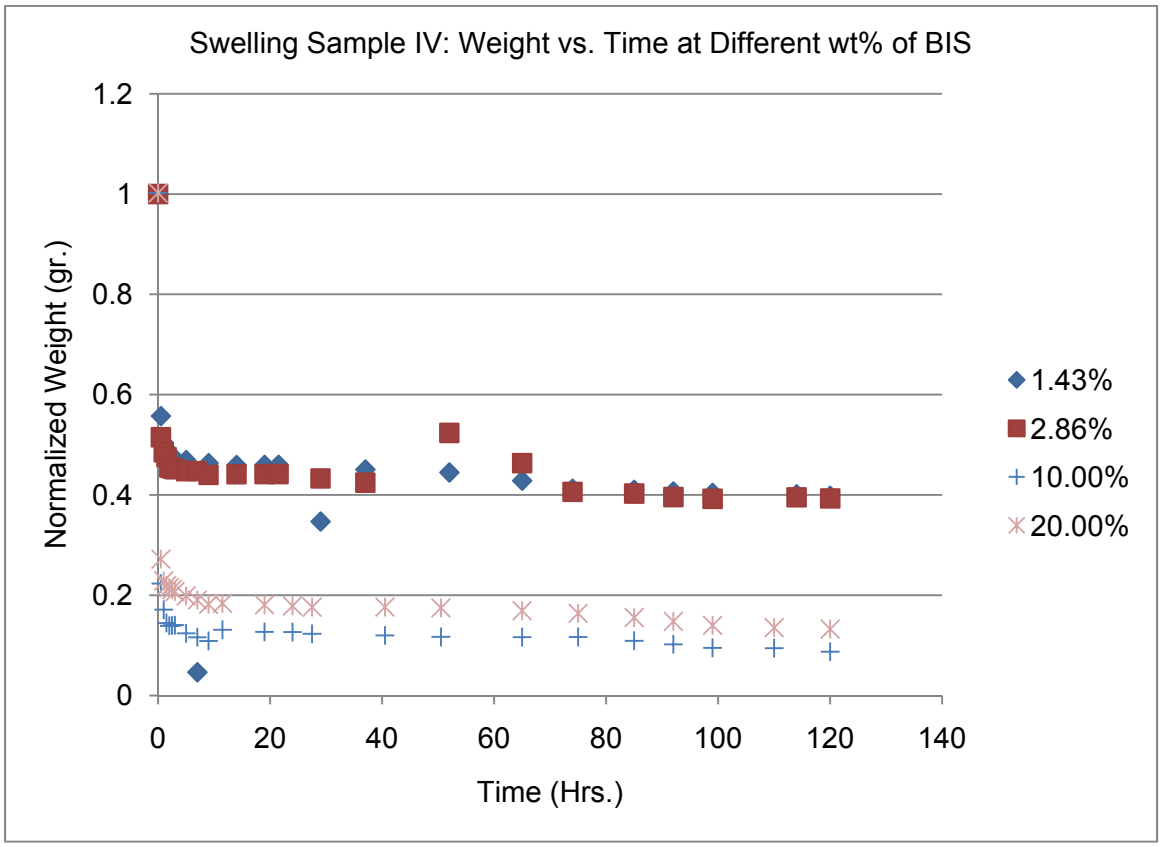

Figure 3-7: Deswelling of 1ml PNIPAAm samples with only four select weight ratios of BIS/NIPAAm shown.

3.3. Crosslink Density Determination

The theory that allows for the determination of the crosslink density based on the swelling limits is the equilibrium swelling theory, which state that a polymer will absorb its neighboring solvent until the solvent chemical potentials inside and outside of the polymer are equal. In terms of osmotic swelling pressure, this can be written as,

$$\Pi_{mix} + \Pi_{elastic} + \Pi_{ion} + \Pi_{elec} = 0 \tag{3.1}$$

It is important to note that this equation makes the assumption that all contribution to the swelling pressure are independent[47]. Here the Π_{mix} is the tendency of the polymer of dissolve into the solvent, $\Pi_{elastic}$ is the elastic response of the network due to crosslinking, Π_{ion} is the contribution to osmotic pressure due to differences in ion concentration between the gel and the water and Π_{elec} is the electrostatic interactions of charges on the polymer chains[47]. Typically the Π_{elec} is very small in comparison to the to Π_{ion} and, for sake of brevity, these will not be discussed at any further length as PNIPAAm is a nonionic polymer and these terms will not be used in its calculations[47].

While theoretical *a priori* calculations can't accurately determine the equilibrium swelling of hydrogels, some theoretical predictions of different parameters of swelling do agree with empirical results. The Flory-Huggins theory defines the mixing contribution by introducing the polymer-solvent interaction parameter (χ_1), as follows:

$$\Pi_{mix} = [RT / V_1][\ln(1-\upsilon_2) + \upsilon_2 + \chi_1 \upsilon_2^2] \tag{3.2}$$

where R is the gas constant, T is absolute temperature, V_1 is the solvent molar volume and υ_2 is the polymer volume fraction[47]. The polymer-solvent interaction parameter takes into account the free energy changes that are caused by mixing and is a function of both temperature and concentration[47]. Its value is typically between 0 and 1, where low values of χ_1 are indicative of good solvents (those that favor minimizing and cause the polymer to swell) and higher values indicate poor solvents (elasticity of the polymer matrix dominates causing the polymer to collapse)[47]. While χ_1 has theoretical backing, it is most often determined empirically and there exist many sources for these values[47, 48]. Heuristics are available for determining χ_1 but since they are inaccurate in systems where hydrogen bonding is significant, it is unlikely they would be a responsible approach for hydrogels[47, 48].

The $\Pi_{elastic}$ term is primarily governed by the elastic restraining forces of the crosslinked polymer chains and is a limiting parameter on extent of swelling[47]. These elastic restraining forces are entropic in nature because stretching of the polymer matrix reduces the number of available chain conformations[47]. For an ideal polymer matrix that is crosslinked in the bulk state, this can be shown as:

$$\Pi_{elastic} = -RT\rho_x[\upsilon_2^{1/3} - 0.5\upsilon^2]. \tag{3.3}$$

If the polymer is prepared in solution, where the chains are in their "relaxed" conformation, equation (3.3) becomes:

$$\Pi_{elastic} = -RT\upsilon_{2,r}\rho_x[(\upsilon_2/\upsilon_{2,r})^{1/3} - 0.5(\upsilon_2/\upsilon_{2,r})] \tag{3.4}$$

where $\upsilon_{2,r}$ is the polymer volume fraction at the time of polymerization[47]. Equation (3.4) reduces back to equation (3.3) in the case that a polymer is not polymerized in the present of the solvent, i.e. $\upsilon_{2,r}$ =1[47].

As stated before, for a nonionic gel, the Flory-Rehner theory represents the total gel pressure as a sum of the osmotic pressure contributions of mixing and elasticity. Combining equations (3.2) and (3.4) we arrive at an equation for the total swelling pressure:

$$[\ln(1-\upsilon_{2,s})+\upsilon_{2,s}+\chi_1\upsilon_{2,s}^{\ 2}]/V_1+\upsilon_{2,r}\rho_x[(\upsilon_{2,s}/\upsilon_{2,r})^{1/3}-0.5(\upsilon_{2,s}/\upsilon_{2,r})] \qquad (3.5)$$

This relationship can easily be solved for the crosslink density from here and is reported to be a good approximation for organic solvents. Because the solvent-interaction parameter cannot account for the hydrogen bonding that will take place in this hydrogel, this calculation of crosslink density stands only as an approximation. Additionally, this calculation assumes that the polymerization goes to completion, which is not always the case.

3.4 Remarks and Results

As expected, the sample without any crosslinker polymerized and exhibited a noticeable change in viscosity but did not congeal and therefore was not included in the swelling test. As for the remaining samples, they calculated crosslink densities are listed below in tables 3-6.

Table 3-6: Crosslink density values (mol/cm^3) calculated from the swelling data using the Flory-Rehner equation.

	Batch			
Sample	1	2	3	4
1	N/A	N/A	N/A	N/A
2	8.11E-09	1.15E-08	3.78E-07	2.33E-07
3	3.63E-06	5.13E-06	3.93E-06	1.27E-06
4	4.26E-05	4.39E-05	4.38E-05	2.73E-05
5	1.33E-04	8.58E-05	1.24E-04	5.99E-05
6	4.21E-04	4.16E-04	3.73E-04	2.28E-04
7	7.56E-04	4.54E-04	1.53E-03	5.55E-04
8	2.76E-04	2.49E-04	1.00E-03	6.58E-04
9	9.10E-04	1.21E-03	1.27E-03	4.45E-04
10	1.56E-03	1.36E-03	2.20E-03	1.38E-03
11	3.72E-03	2.50E-03	2.37E-03	7.12E-04
12	2.06E-03	2.79E-03	4.09E-03	2.93E-03
13	2.05E-03	2.80E-03	1.43E-03	1.83E-03
14	6.89E-03	3.82E-03	1.42E-03	7.12E-04
15	3.89E-03	3.47E-03	1.45E-03	1.15E-03

In order to makes these calculations, an interaction parameter of 0.5 and a dry density of 1.37 g/cm^3 were used to solve the Flory-Rehner equation[49-51].

There is a significant swelling difference (~60%) between samples created with the acetone rich recipe and the intended 25/75 mix. Plots of swelling and deswelling kinetics are displayed in figures 3-2 through 3-17. A possible explanation for this may be that the additional water present is enough to have a swelling effect on the PNIPAAm

samples as they are polymerizing. This swelling would limit chain conformations and subsequently hinder network formation. Hence, the water rich system would be less developed and not capable of swelling to the same magnitude as the acetone rich sample.

Additional variability in the data is likely the result of structural defects that occurred during deswelling. Upon deswelling some samples, typically those with the lowest crosslink density formed an opaque skin inhibited deswelling, while other fractured across the top or along multiple planes, expediting deswelling. These two effects are shown in figures 3-18 and 3-19.

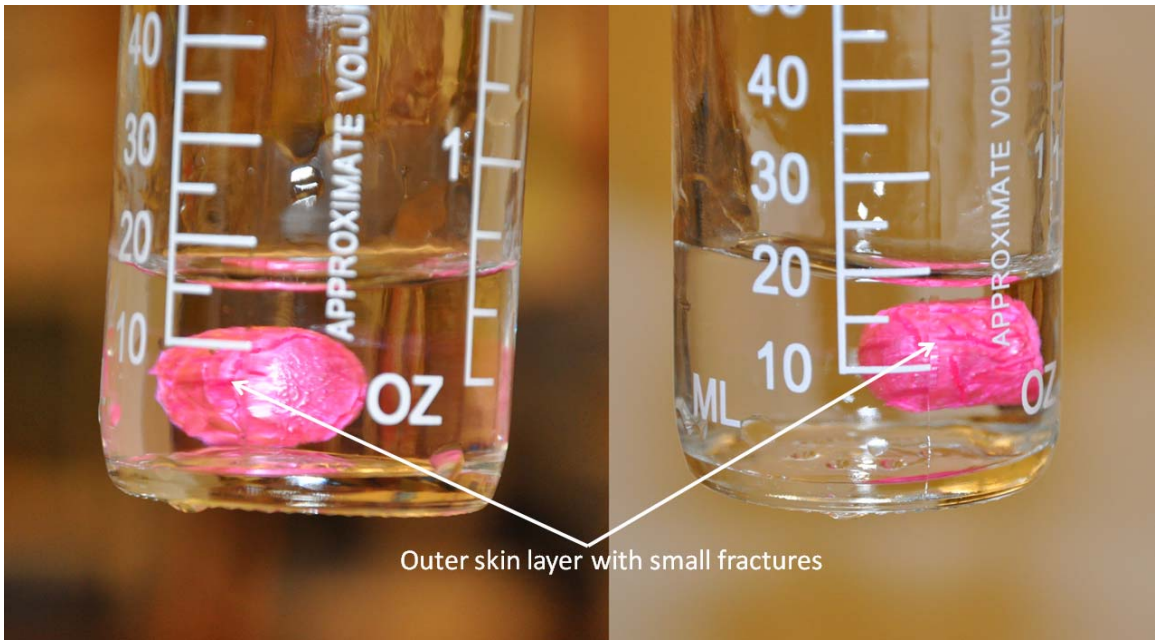

Figure 3-8: Collapsing gel that forms an outer skin layer.

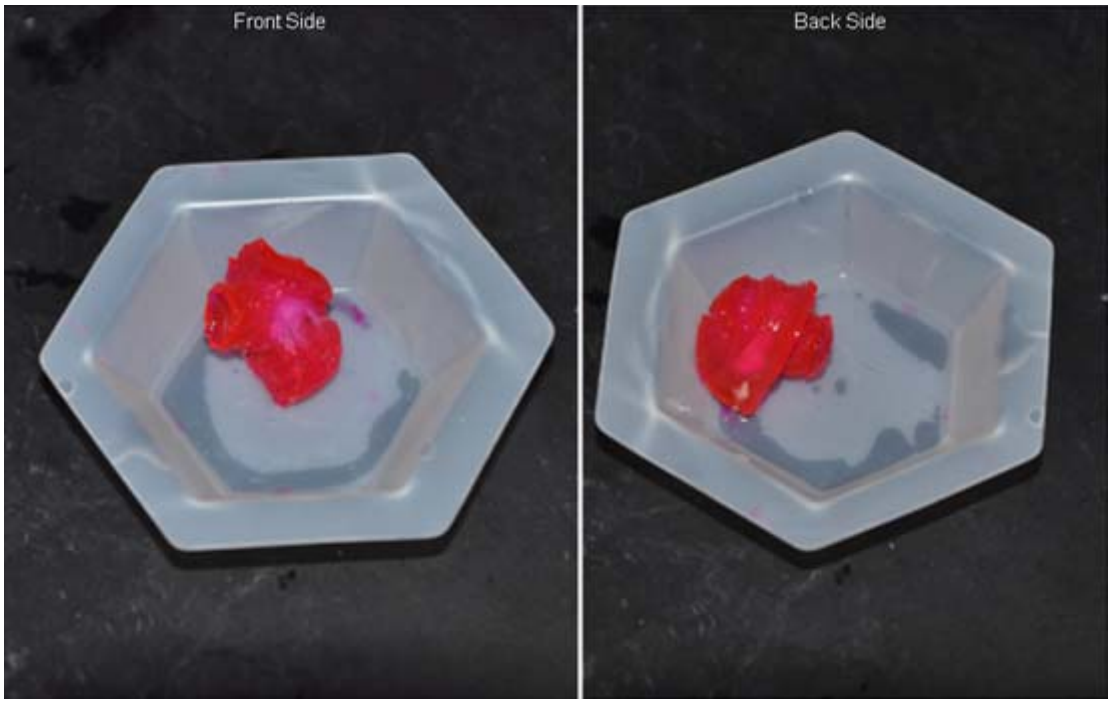

Figure 3-9: A PNIPAAm that fractured in the process of swelling.

Also, the swelling data collected has confirmed that there are only small changes in the extent of swelling or in swelling kinetics when the crosslinker concentration is beyond 5-7 wt% BIS/NIPAAm. Therefore, investigating the swelling properties of these densities is of little worth to the nature of this work, as these gels aren't likely to swell enough to enter a deformation regime.

CHAPTER FOUR: CHARACTERIZATION OF CONFORMATION OF PNIPAAm MICROSTRUCTURES BY LASER SCANNING CONFOCAL MICROSCOPY

4.1. Laser Scanning Confocal Microscopy Introduction

Wide-field fluorescence microscopy is commonly used for the investigation of organic or inorganic substances on a micron or submicron range by using florescence or phosphorescence phenomena, as opposed to adsorption and reflection[52]. It operates by evenly irradiating the sample with light and exciting those portions of the sample simultaneously causing it to fluoresce[52]. The emitted fluorescence is captured by photodetectors or cameras and then translated into a coherent image[52]. This method is limited by the microscopes ability to filter out background information, concisely control the depth of field and collect optical sections of thicker specimens[53]. These are the exact limitation that Marvin Minsky sought to overcome in the 1950's when he invented confocal microscopy.

In contrast to fluorescence microscopy, confocal microscopy uses pin-point illumination and a pinhole aperture that is positioned in the conjugate plane (confocal) with the illumination point on the specimen and a second pinhole aperture in front of the detector (a photomultiplier tube)[53]. A schematic of the confocal microscope setup and a comparison of wide field vs confocal illumination volumes can be seen in figures 4-1 and 4-2. Once the laser is emitted it is reflected by the chromatic mirror and rastered across a specific focal plane of the specimen where it excites secondary fluorescence and sends light back through the dichromatic mirror to the detector pinhole aperture, filtering out-of-focus or out-of-plane light and propagating all other light to the

photomultiplier detector[53]. With the out-of-focus light excluded from the emissions data, a more accurate account of the specimen can be rendered.

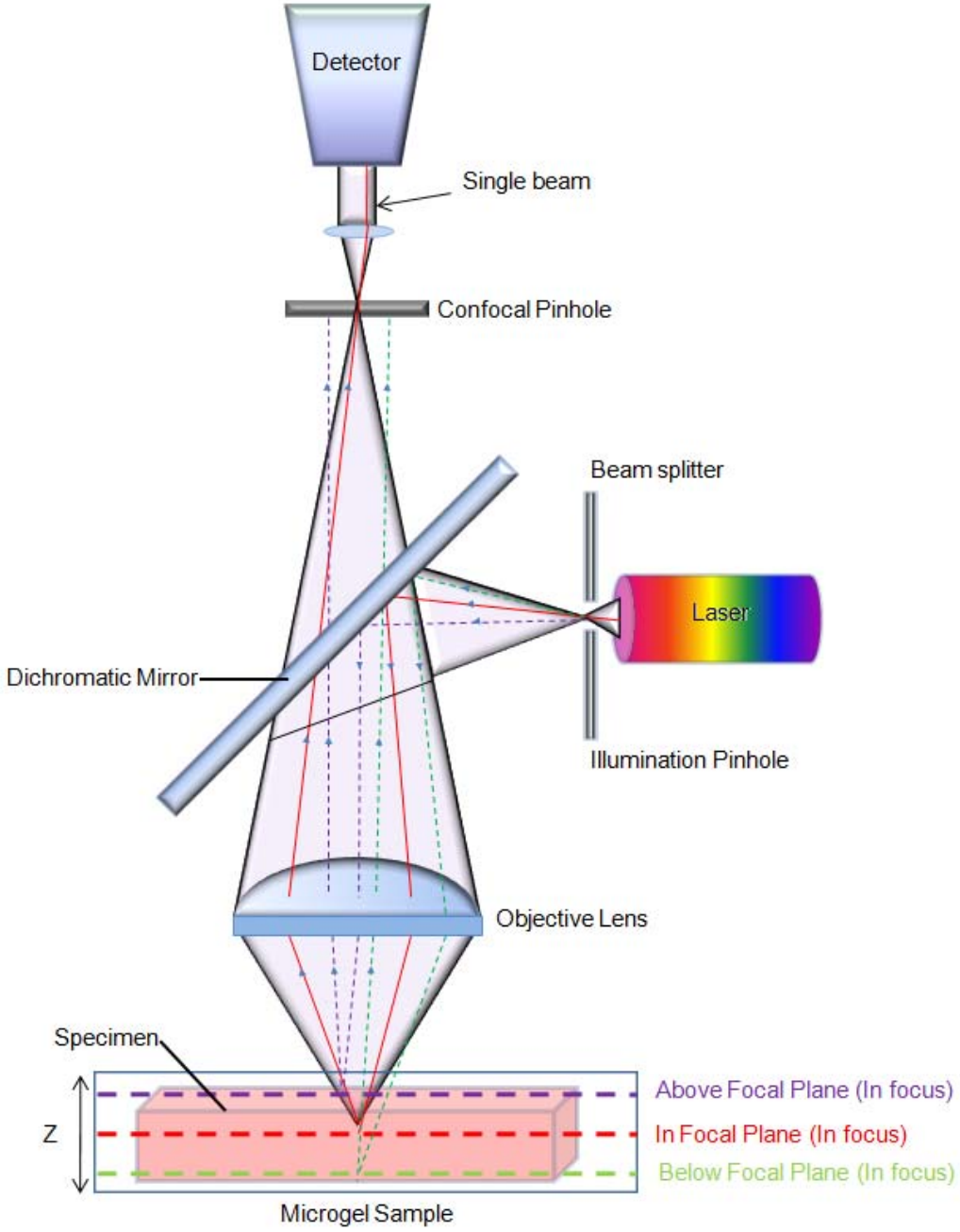

Figure 4-1: A schematic of the confocal microscope concept.

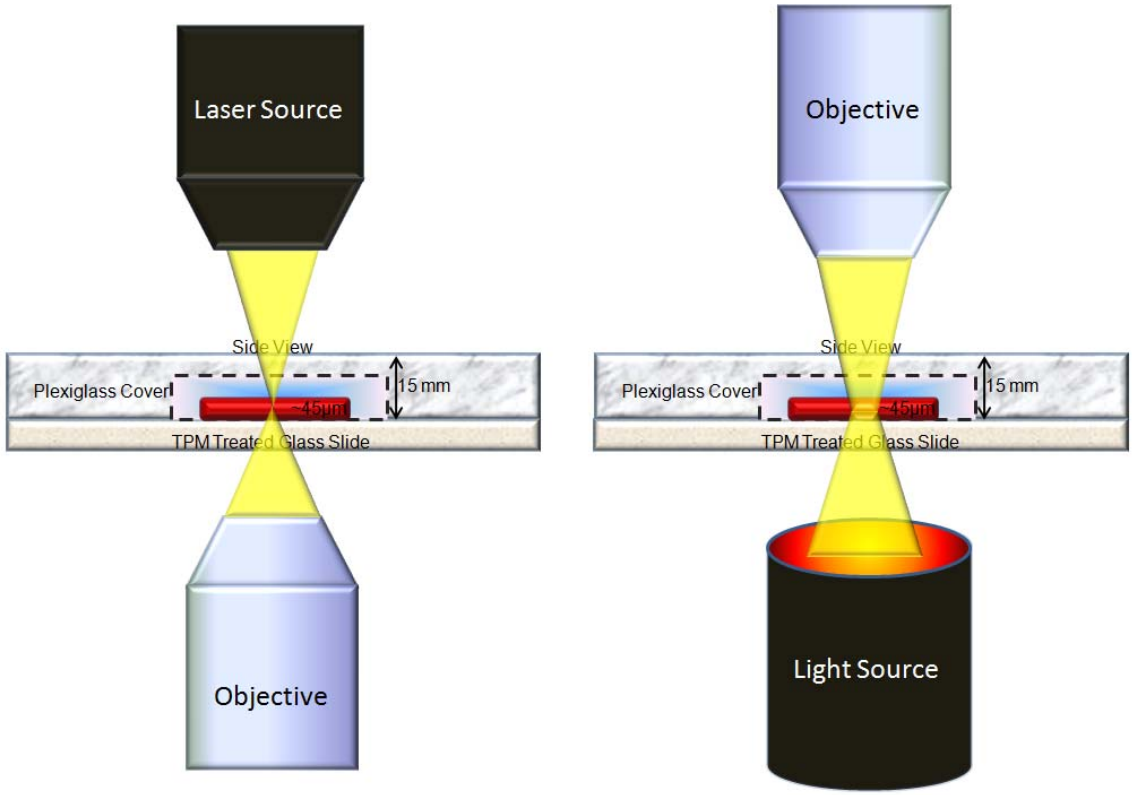

Figure 4-2: Difference in illumination volume between wide-field and confocal microscopy.

On the downside, confocal microscopy is limited by the number of excitation wavelengths that are available by today's lasers, which emit relatively narrow bands and are costly (especially in the UV spectrum)[53]. Concurrently, the high price of purchasing and operating a confocal microscope limits the number of facilities that can afford one[53]. Also, the high intensity lasers that are used in laser scanning microscopy can be harmful to living cells or organism[53]. This problem was circumvented by Nipkow disk confocal microscopy by using a multiphoton source at lower intensities but since this is neither a limitation to the current investigation nor an technique employed, this will not be discussed further[53].

4.2. Characterization of Structural Morphology by Confocal Microscopy

The images take with the scanning laser confocal microscope are individual slices or well-defined planes within a sample[53]. These may be taken from the x-y, x-z, or y-z planes over some desired thickness. Additionally, if an area of interest (AOI) is greater that the scan area, the boundaries of this AOI may be entered into the software interface and the microscope will split the AOI into separate image stacks that can then be fused together to form the larger AOI.

The micrographs shown have been taken with a Leica TCS SP5 confocal laser scanning microscope (CLSM) through a 20X/0.7NA (Leica Microsystems, Germany). An Argon laser line with an emission at 543 nm was used to excited the fluorescent microstructures and an AOBS was used to filter the images. The images were recorded with photomultiplier detectors using LAS AF software (version 2.1.0, Leica Microsystems, Germany). Image stack were taken at z-steps (thickness spacing) between 0.25 and 1 μm.

The 3-D images of the PNIPAAm microstructures were rendered using Imaris 5.5.0 (Bitplane, Inc., St. Paul, Minnesota) software package. The RAW data from the scanning confocal microscope was imported into Imaris and then refined using the software's thresholding ability to remove background fluorescence. From here the individual stacks were assembled to create and iso-surface of the microgel.

4.3. Remarks and Results

Because of the inherent inaccuracies that come with adhering glass slides to Plexiglass covers with nail polish, samples have often been displacement between opposite ends that measure as much as 40 μm. Unfortunately, an AOI that runs

diagonally through a sample requires that the number of scan slice be increased to capture the data and the user must deal with the excess data. An illustration of this drawback is displayed in figure 4-3.

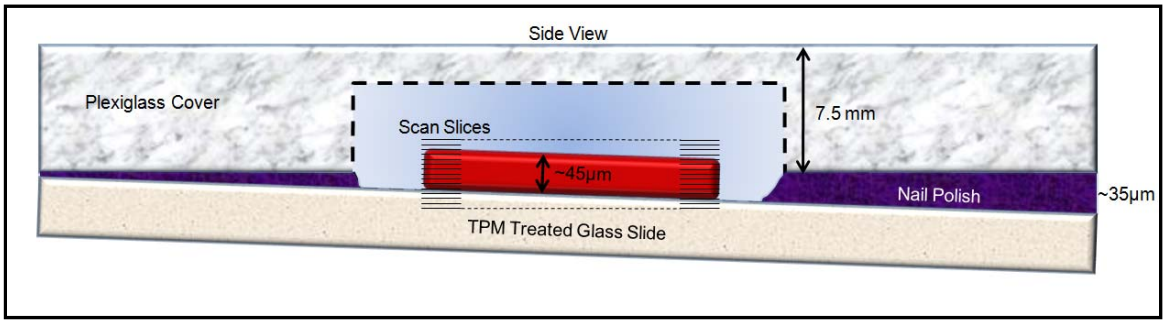

Figure 4-3: Increased number of stacks to compensate for uneven adhesive layer.

To this point, all PNIPAAm monolithe structures have been made using the first recipe (i.e. the one that uses pure acetone for dilution) for varying BIS concentrations and all resulting structures have exhibited sharply angled side-walls accompanied by deep concavities across the width. This concavity yield structural edges that vary along the monolithe between 15 µm and 18 µm on average and concave valleys that run the length of the structure and are an average of ~10 µm in height, as displayed in figure 4-4. A thinner portion of the stack, about 20 µm in width, looks closer to what has been seen in the past but is $<1/5^{th}$ the height of the mold. This is show in figure 4-5. The swollen states of both of these also yield unusual findings. While they both exhibit the expected deformations, there are small nuances that do not follow with previous observation. The low aspect ratio structure displays edge undulation but the effect is less pronounced than usual and higher aspect ratio end buckles but the structural bulge that is often present on the outside of the wave is now pronounce on the inside. Both of these structures are show in figures 4-6 and 4-7.

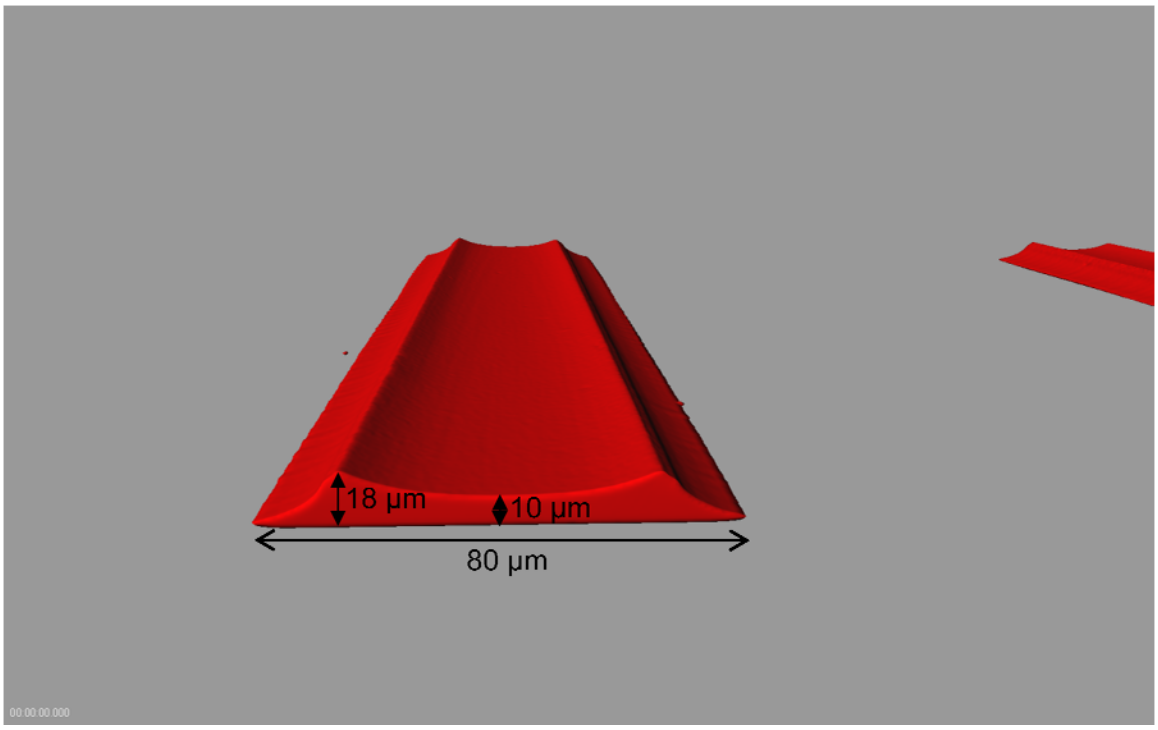

Figure 4-4: PNIPAAm monolith in the collapsed state.

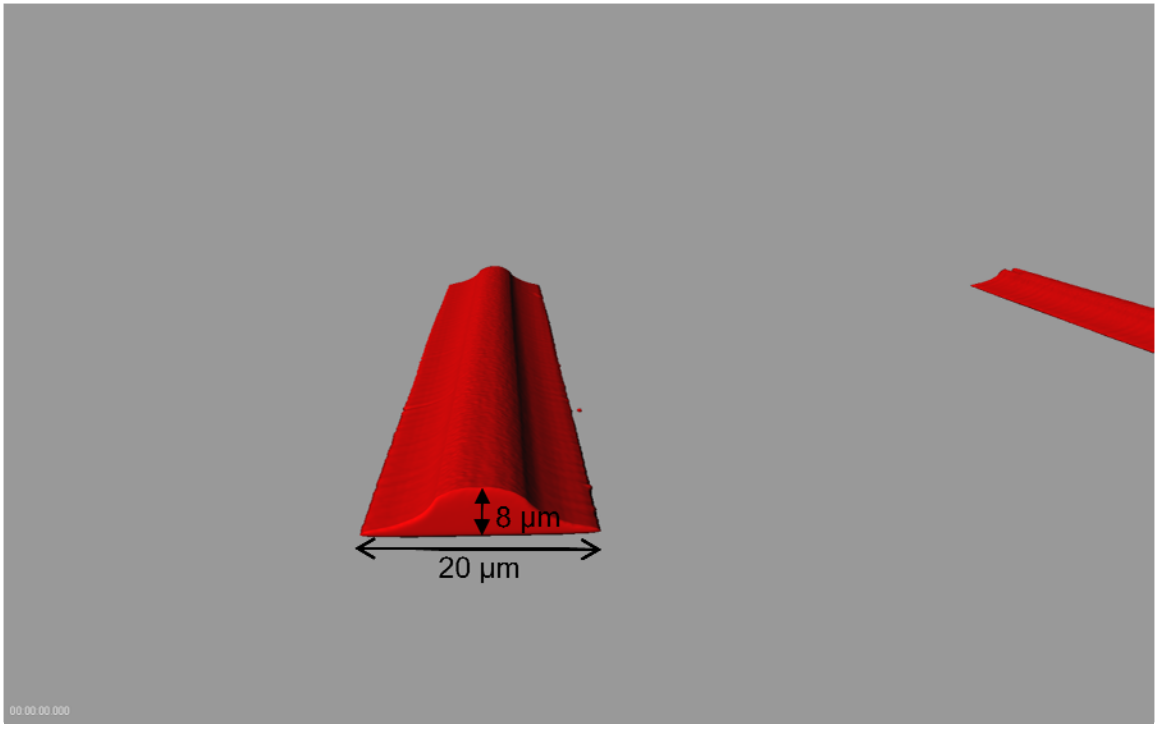

Figure 4-5: PNIPAAm monolith in the collapsed state.

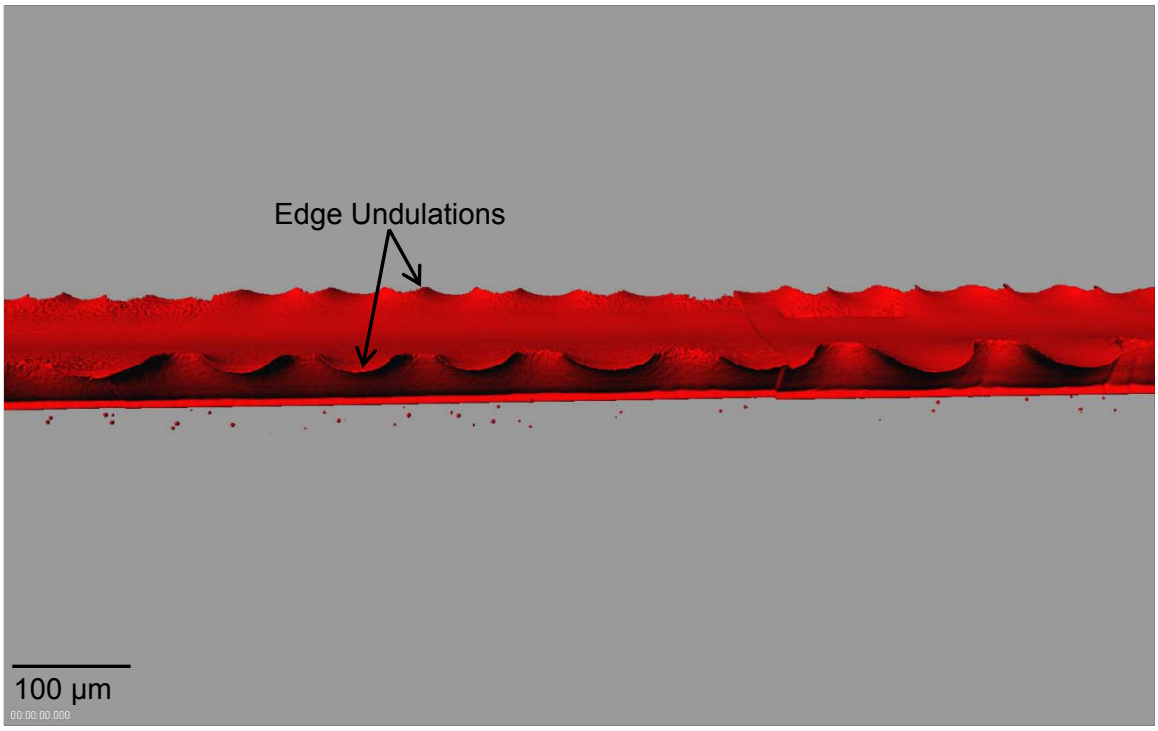

Figure 4-6: PNIPAAm monolith exhibiting surface deformations in the swollen state.

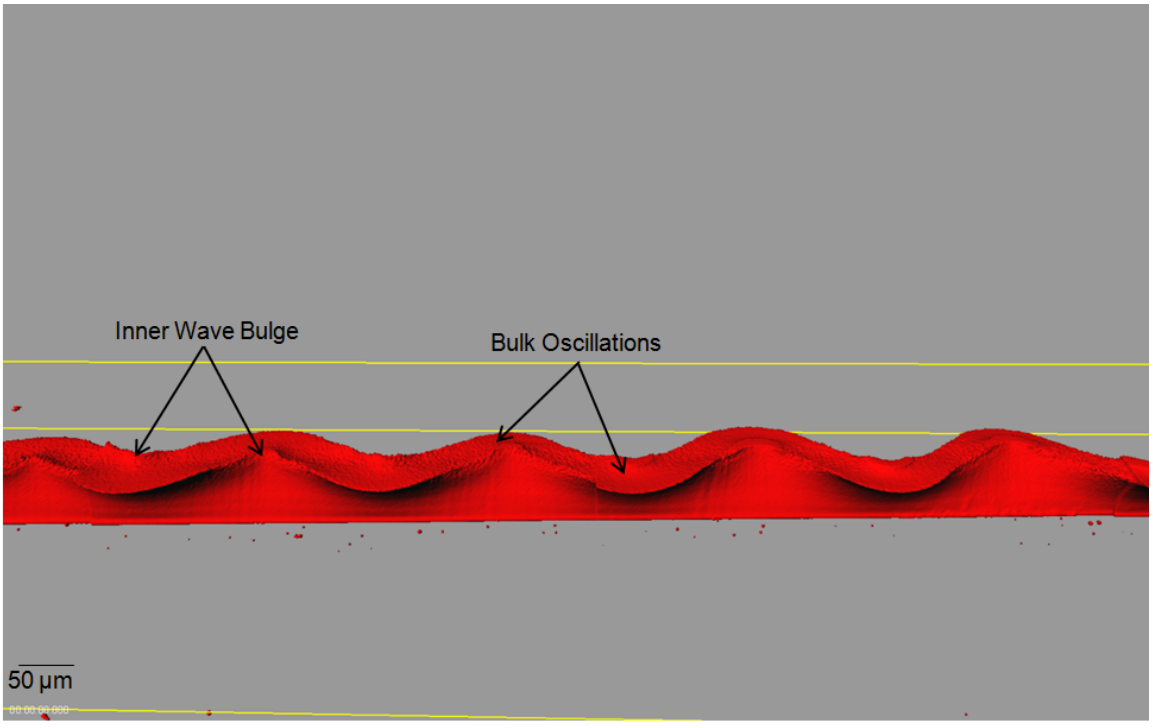

Figure 4-7: PNIPAAm monolith exhibiting bulk mechanical deformation in the swollen state.

Structures of this nature have only been observed using the variable BIS recipes described herein and have not been observed using original solution recipes. It is currently believed that the observed effect is the result of increased surface tension of the prepolymer solution that results in a meniscus or some other phenomena when applied to mimic. To this point, all other potential causes (PMDS or SU-8 height and PNIPAAm being torn off) have been disproven.

CHAPTER FIVE: SUMMARY, CONCLUSION AND FUTURE WORK

This study has examined the techniques used to reproducible construct surface-confined Poly(N-isoropylacrylamide) microgels, measure crosslink density of these gels and how to characterize their buckling behavior in real time with the use of confocal microscopy. Many challenges were faced in these endeavors and these trials and triumphs will be covered here. Lastly, current and future approaches for establishing correlations between crosslink density and mechanical deformations will be discussed.

5.1. Preparing Stock Solutions

Ultimately, using a suspended solution and a stir plate is not the most ideal approach but is suitable for the nature of this swelling test. A more analytical approach should be sought out to eliminate sources of potential error that are eminent with this approach. These source might include, changing BIS concentration over time due to the high volatility of the solvent, recrystallization of BIS along the edges of the container due to the volatility of this mixture and its supersaturated nature, and the error in samples taken when the stock is intermittently remove from the stir plate and allow to stop mixing before withdraw. Moreover, this method was used out of convenience and necessity of time.

5.2. Sample Preparation

There may be a small loss in accuracy when samples were removed by fracturing the culture tubes if the samples are marred in any way. When this approach was used, it was done with the utmost care to avoid such incidents.

5.3. Experimental Setup and Data Collection

It is important to handle these samples with care as they are dried and weighed each time. It was found in the “beta test” (not included in the 4 batches listed herein), that dropping samples or picking this up with one’s fingers, were likely to result in a fractured sample. This made the remaining data collection very toilsome and the data less accurate.

Additionally, the beta test revealed that samples should be thoroughly collapsed before they are sent to dry in the vacuum furnace or they run the risk of exploding. Extra care was taken to avoid this.

5.4. Confocal Microscopy

These image stacks can also be take repeatedly over time. The 4-D data can allow for the in-situ view of PNIPAAm structures, as they transition from collapsed to swollen or vice-versa. However, due to the relative speed/quality of the resulting image stacks, changes may out-pace the raster ability. To overcome this, the nature of the solvent (water) can be changed by added salts. Do so allows for a step by step transformation of the PNIPAAm structures and allows for high-resolution image stack to be acquired at each stage. This technique is currently being employed to study the relationship between crosslink density and buckling conformations.

5.5. Future Works

5.5.1. Soft Lithography

A mentioned drawback to the MIMIC technique is that it requires the molding stamp patterns to have attached corridors through which the prepolymer solution may flow. With this technique, patterns without these fluid ducts can be achieved however this must be done through manual cleaving of the ducts after the polymer is formed. Since this is both in accurate and potentially damaging to the PNIPAAm structure, other soft lithography methods need to be investigate. Additionally, there are several patters on “Monolithe II” that would support such a technique and the methods for its application are well established. This could potentially give rise to free-standing, actuatable surfaces depressions for capturing or storing, free-standing monolithes and surfaces mimicking biological smooth muscle[54, 55].

5.5.2. Preparing Stock Solutions

In light of some of the drawbacks mentioned above, future stock solutions will be prepared in a more analytical fashion. Instead of pipetting from a suspension of the crosslinker, excess solvent will be used to fully solvate the mass of BIS needed in the respective recipe and then evaporated off. The solvent required for this aliquot can be added in after the fact and will allow for the entire process to take place inside of the glove bag. Adding this extra solvent to the NIPAAm stock solution would also help with lower its propensity to crystallize on the edges of the stock container.

5.5.3. Confocal Microscopy Characterization

Additional characterization still needs to be done to determine the effect that crosslink density has on surface confined structures and buckling morphologies. These structural conformations will be further studied and used to valid or disprove current elastic theory of surface confined hydrogels.

REFERENCES

[1] J.P. Rolland, B.W. Maynor, L.E. Euliss, A.E. Exner, G.M. Denison, J.M. DeSimone, Direct Fabrication and Harvesting of Monodisperse, Shape-Specific Nanobiomaterials, Journal of the American Chemical Society 127 (2005) 10096-10100.

[2] A. Dongshin Kim, J.B.A. David, Lab on a Chip Hydrogel-based reconfigurable components for microfluidic devices, 2006.

[3] M.E. Harmon, M. Tang, C.W. Frank, A microfluidic actuator based on thermoresponsive hydrogels, Polymer 44 (2003) 4547-4556.

[4] Q. Luo, S. Mutlu, Y.B. Gianchandani, F. Svec, J.M.J. Fréchet, Monolithic valves for microfluidic chips based on thermoresponsive polymer gels, Electrophoresis 24 (2003) 3694-3702.

[5] J. Wang, Z. Chen, M. Mauk, K.-S. Hong, M. Li, S. Yang, H. Bau, Self-Actuated, Thermo-Responsive Hydrogel Valves for Lab on a Chip, Biomedical Microdevices 7 (2005) 313-322.

[6] A. Castellanos, S.J. DuPont, A.J. Heim, G. Matthews, P.G. Stroot, W. Moreno, R.G. Toomey, Size-Exclusion "Capture and Release" Separations Using Surface-Patterned Poly(N-isopropylacrylamide) Hydrogels, Langmuir 23 (2007) 6391-6395.

[7] L.K. Ista, V.H. Perez-Luna, G.P. Lopez, Surface-Grafted, Environmentally Sensitive Polymers for Biofilm Release, Appl. Environ. Microbiol. 65 (1999) 1603-1609.

[8] M. Ebara, J.M. Hoffman, P.S. Stayton, A.S. Hoffman, Surface modification of microfluidic channels by UV-mediated graft polymerization of non-fouling and 'smart' polymers, Radiation Physics and Chemistry 76 (2007) 1409-1413.

[9] Y. Hirokawa, T. Tanaka, Volume phase transition in a nonionic gel, The Journal of Chemical Physics 81 (1984) 6379-6380.

[10] M. Shibayama, T. Tanaka, Volume phase transition and related phenomena of polymer gels, Responsive Gels: Volume Transitions I, 1993.

[11] H.G. Schild, Poly(N-isopropylacrylamide): experiment, theory and application, Progress in Polymer Science 17 (1992) 163-249.

[12] P.J. Flory, J.J. Rehner, Statistical Mechanics of Cross-Linked Polymer Networks II. Swelling, The Journal of Chemical Physics 11 (1943) 521-526.

[13] P.J. Flory, J.J. Rehner, Statistical Mechanics of Cross-Linked Polymer Networks I. Rubberlike Elasticity, The Journal of Chemical Physics 11 (1943) 512-520.

[14] A. Vidyasagar, J. Majewski, R. Toomey, Temperature Induced Volume-Phase Transitions in Surface-Tethered Poly(N-isopropylacrylamide) Networks, Macromolecules 41 (2008) 919-924.

[15] R. Toomey, D. Freidank, J. Ruhe, Swelling Behavior of Thin, Surface-Attached Polymer Networks, Macromolecules 37 (2004) 882-887.

[16] S. Seelenmeyer, I. Deike, S. Rosenfeldt, C. Norhausen, N. Dingenouts, M. Ballauff, T. Narayanan, P. Lindner, Small-angle x-ray and neutron scattering studies of the volume phase transition in thermosensitive core--shell colloids, The Journal of Chemical Physics 114 (2001) 10471-10478.

[17] S.J. DuPont, Swelling-Induced Instabilities in Surface-Confined Poly(N-isopropylacrylamide) Microgels, Soft Matter (In Review).

[18] T. Mora, A. Boudaoud, Buckling of swelling gels, Eur. Phys. J. E 20 (2006) 119-124.

[19] R.C. Hayward, B.F. Chmelka, E.J. Kramer, Template Cross-Linking Effects on Morphologies of Swellable Block Copolymer and Mesostructured Silica Thin Films, Macromolecules 38 (2005) 7768-7783.

[20] T. Tanaka, S.-T. Sun, Y. Hirokawa, S. Katayama, J. Kucera, Y. Hirose, T. Amiya, Mechanical instability of gels at the phase transition, Nature 325 (1987) 796-798.

[21] W. Hong, Z. Liu, Z. Suo, Inhomogeneous swelling of a gel in equilibrium with a solvent and mechanical load, International Journal of Solids and Structures 46 (2009) 3282-3289.

[22] M.A. Biot, Exact Theory of Buckling of a Thick Slab, Appl. sci. Res. 20 (1963) 5.

[23] H. Inomata, N. Wada, Y. Yagi, S. Goto, S. Saito, Swelling behaviours of N-alkylacrylamide gels in water: effects of copolymerization and crosslinking density, Polymer 36 (1995) 875-877.

[24] K.F. Freed, A.I. Pesci, Computation of the crosslink dependence of the effective Flory interaction parameter .chi. for polymer networks, Macromolecules 22 (1989) 4048-4050.

[25] S.H. Gehrke, M. Palasis, M.K. Akhtar, Effect of synthesis conditions on properties of poly(N-isopropylacrylamide) gels, Polymer International 29 (1992) 29-36.

[26] P.A. Clerc, et al., Advanced deep reactive ion etching: a versatile tool for microelectromechanical systems, Journal of Micromechanics and Microengineering 8 (1998) 272.

[27] Y. Hanein, C.G.J. Schabmueller, G. Holman, uuml, P. cke, D.D. Denton, ouml, K.F. hringer, High-aspect ratio submicrometer needles for intracellular applications, Journal of Micromechanics and Microengineering 13 (2003) S91-S95.

[28] Y. Xia, G. Whitesides, SOFT LITHOGRAPHY, Annual Review of Materials Science 28 (1998) 153-184.

[29] Piranha etch | University of British Columbia's AMPEL Nanofabrication and Microfabrication Facility, University of British Columbia's AMPEL Nanofabrication and Microfabrication, 2010.

[30] M.C. Hull, L.R. Cambrea, J.S. Hovis, Infrared Spectroscopy of Fluid Lipid Bilayers, Analytical Chemistry 77 (2005) 6096-6099.

[31] K.J. Seu, A.P. Pandey, F. Haque, E.A. Proctor, A.E. Ribbe, J.S. Hovis, Effect of Surface Treatment on Diffusion and Domain Formation in Supported Lipid Bilayers, Biophysical Journal 92 (2007) 2445-2450.

[32] SU-8 2000 Permanenet Epoxy Negative Photoresist, MicroChem, 2009.

[33] Y.J. Chuang, F.G. Tseng, W.K. Lin, Reduction of diffraction effect of UV exposure on SU-8 negative thick photoresist by air gap elimination, Microsystem Technologies 8 (2002) 308-313.

[34] A. Revzin, R.J. Russell, V.K. Yadavalli, W.-G. Koh, C. Deister, D.D. Hile, M.B. Mellott, M.V. Pishko, Fabrication of Poly(ethylene glycol) Hydrogel Microstructures Using Photolithography, Langmuir 17 (2001) 5440-5447.

[35] X.-M. Zhao, Soft lithographic methods for nano-fabrication, J. Mater. Chem. 7 (1997) 6.

[36] A.D. Stroock, S.K.W. Dertinger, A. Ajdari, I. Mezic, H.A. Stone, G.M. Whitesides, Chaotic Mixer for Microchannels, Science 295 (2002) 647-651.

[37] J.M.K. Ng, I. Gitlin, A.D. Stroock, G.M. Whitesides, Components for integrated poly(dimethylsiloxane) microfluidic systems, ELECTROPHORESIS 23 (2002) 3461-3473.

[38] H. Takao, K. Miyamura, H. Ebi, M. Ashiki, K. Sawada, M. Ishida, A MEMS microvalve with PDMS diaphragm and two-chamber configuration of thermo-pneumatic actuator for integrated blood test system on silicon, Sensors and Actuators A: Physical 119 (2005) 468-475.

[39] E. Delamarche, H. Schmid, B. Michel, H. Biebuyck, Stability of molded polydimethylsiloxane microstructures, Advanced Materials 9 (1997) 741-746.

[40] A.W. Feinberg, A. Feigel, S.S. Shevkoplyas, S. Sheehy, G.M. Whitesides, K.K. Parker, Muscular Thin Films for Building Actuators and Powering Devices, Science 317 (2007) 1366-1370.

[41] B.H. Jo, L.M. Van Lerberghe, K.M. Motsegood, D.J. Beebe, Three-dimensional micro-channel fabrication in polydimethylsiloxane (PDMS) elastomer, Journal of Microelectromechanical Systems 9 (2000) 76-81.

[42] D. Qin, Y. Xia, J. Rogers, R. Jackman, X.-M. Zhao, G. Whitesides, Microfabrication, Microstructures and Microsystems, Microsystem Technology in Chemistry and Life Science, 1998, pp. 1-20.

[43] R. Banga, J. Yarwood, A.M. Morgan, B. Evans, J. Kells, FTIR and AFM Studies of the Kinetics and Self-Assembly of Alkyltrichlorosilanes and (Perfluoroalkyl)trichlorosilanes onto Glass and Silicon, Langmuir 11 (1995) 4393-4399.

[44] P. Silberzan, L. Leger, D. Ausserre, J.J. Benattar, Silanation of silica surfaces. A new method of constructing pure or mixed monolayers, Langmuir 7 (1991) 1647-1651.

[45] J.B. Brzoska, I.B. Azouz, F. Rondelez, Silanization of Solid Substrates: A Step Toward Reproducibility, Langmuir 10 (1994) 4367-4373.

[46] M.J. Park, W.M. Choi, O.O. Park, Patterning polymer light-emitting diodes by micromolding in capillary, Current Applied Physics 6 (2006) 627-631.

[47] L. Brannon-Peppas, Absorbent Polymer Technology, Elsevier Publishing Company, Amsterdam, 1990.

[48] A.F.M. Barton, Handbook of Solubility Parameters and Other Cohesion Parameters, CRC Press, Boca Raton, 1983.

[49] H. Feil, Y.H. Bae, J. Feijen, S.W. Kim, Effect of comonomer hydrophilicity and ionization on the lower critical solution temperature of N-isopropylacrylamide copolymers, Macromolecules 26 (1993) 2496-2500.

[50] K. Tauer, D. Gau, S. Schulze, A. Völkel, R. Dimova, Thermal property changes of poly(N-isopropylacrylamide) microgel particles and block copolymers, Colloid & Polymer Science 287 (2009) 299-312.

[51] A.K. Lele, M.M. Hirve, M.V. Badiger, R.A. Mashelkar, Predictions of Bound Water Content in Poly(N-isopropylacrylamide) Gelâ€ Macromolecules 30 (1997) 157-159.

[52] B. Herman., Fluorescence microscopy, 2nd ed. ed., Oxford, UK : Bios Scientific Publishers ; New York : Springer in Association with the Royal Microscopical Society, 1998.

[53] F.T.J. Claxton N S, Davidson M W., Laser scanning confocal microscopy, 2008.

[54] D.E. Ingber, Mechanical control of tissue growth: Function follows form, PNAS 102 (2005) 11571-11572.

[55] E. Armstrong, A. Schleicher, H. Omran, M. Curtis, K. Zilles, The Ontogeny of Human Gyrification, Cereb. Cortex 5 (1995) 56-63.